

國立臺灣大學生農學院森林環境暨資源學研究所

博士論文

School of Forestry and Resource Conservation

College of Bio-resources and Agriculture

National Taiwan University

Doctoral Dissertation

應用遙測技術於臺灣北部地區水文循環之研究

Study on the Hydrologic Cycle of the Northern Taiwan

Using Remote Sensing Techniques

吳治達

Chih-Da Wu

指導教授：羅漢強 博士

鄭祈全 博士

Advisor: Hann-Chung Lo, Ph.D.

Chi-Chuan Cheng, Ph.D.

中華民國 99 年 4 月

April, 2010

國立臺灣大學博士學位論文
口試委員會審定書

應用遙測技術於臺灣北部地區水文循環之研究
Study on the Hydrological Cycle of the Northern Taiwan
Using Remote Sensing Techniques

本論文係吳治達君 (d94625002) 在國立臺灣大學森林環境暨資源學研究所完成之博士學位論文，於民國 99 年 4 月 9 日承下列考試委員審查通過及口試及格，特此證明

口試委員：

羅漢強 鄭新全

(簽名)

(指導教授)

陳朝川

詹進發

林金樹

洪永寬

許立達

系主任、所長

羅漢強 (簽名)

(是否須簽章依各院系所規定)



謝 誌

光陰荏苒，自研究所起算，轉瞬間在台大已度過了七年的時光，隨著求學生涯即將暫告一段落，心中湧現的，是對於過程中眾人的支持無限的感恩。

本論文承蒙恩師 羅漢強教授及 鄭祈全教授之引導啟發，求學期間兩位恩師不時指導學生正確的方向，並於研究架構與內容惠賜卓見、逐字匡正，論文始能順利付梓，內心感恩之情，難以言喻，謹誌卷首，以申謝忱。

論文初稿，復蒙屏東科技大學陳朝圳副校長、銘傳大學觀光學院陳永寬院長、嘉義大學森林暨自然資源學研究所林金樹主任、政治大學地政學研究所詹進發副教授、文化大學森林暨自然保育學系許立達副教授詳予審閱口試，匡正謬誤，惠賜卓見，使本文更臻完善，衷心感謝。

衷心感謝恩師嘉義大學森林暨自然資源學研究所 林金樹主任及 林喻東老師不斷之教導與鼓勵，引領學生進入森林經營與遙感探測之研究領域，學生始得完成碩士及博士學業，老師栽培之苦心，學生永銘在心。

感謝美國愛達荷州立大學研究發展中心 Rick Allen 博士於程式撰寫上之協助；美國國家職業安全衛生中心 Lynda M. Ewers 博士在論文文法及用詞上之逐字匡正；屏東科技大學森林系陳朝圳老師及鐘玉龍老師於分析程式及材料上之提供；台灣大學生物環境系統工程學系童慶斌老師於分析程式上之提供；內政部國土測繪中心於國土利用調查資料之提供，使論文能順利完成，謹致上最誠摯之謝意。

研究期間，感謝焦國模老師及陳永寬老師在航、遙測方面的啟蒙，以及日常生活及為人處世方面之諸多指導；羅漢強老師及鄭祈全老師於課業上之指點；政治大學詹進發老師於研究架構上之指導；彰化師範大學王素芬老師於集水區生態學方面多所指正；師母范秀蘭女士在各方面的照顧及協助；葉堃生學長、鄧淑萍學姐、吳耀楠學長、學妹施瑩瑄及陳奐閱之多方鼓勵；同窗好友，加拿大英屬哥

倫比亞大學莊永忠博士後研究員在求學期間的同甘共苦，相互勉勵；政治大學地政學系遙測實驗室的彥廷、阿瑪、郁晴、幸宜、奧莉薇、安勤、清智、曉彤，你們的幫忙及搞笑，均是難以忘懷之回憶，在此致上無盡的謝意。

感謝全家人及父母多年來的支持，使我得以在學術研究上全力衝刺，無後顧之憂；此外，摯友慧如多年來不離不棄，默默支持，一路相伴，更是我前進的動力，沒有妳的體諒、包容，相信這七年的生活將是很不一樣的光景。

最後，謹以此文獻給曾經幫助過我的所有人。

吳治達 謹識於

台灣大學森林環境暨資源學研究所森林攝影測量研究室

中華民國 99 年 4 月



中文摘要

環境變遷與集水區水文循環之間的關係已成為環境規劃的重要課題。國內外已有許多專家學者結合大氣環流模式 (General Circulation Models, GCMs) 與 GWLF 河川流量模式 (Generalized Watershed Loading Functions, GWLF)，探討氣候變遷對集水區水資源的衝擊效應。但大部份的研究除受限於大尺度地表蒸發散量的調查不易之外，在蒸發散覆蓋係數 (Evapotranspiration Cover Coefficient, CV) 之設定方面，亦大多根據 GWLF 手冊中所列之參考值進行設定。然真實地表之土地使用類別甚為複雜，如僅依手冊中之參考值進行參數設定，可能會影響分析結果之正確性。此外，土地使用型態和蒸發散量的逐年變化，亦會影響集水區之未來水文狀態，而傳統的流量模擬研究甚少針對此兩項因子之影響效應加以探討。

有鑑於此，本研究以台灣北部地區為試區，旨在利用遙測技術推估真實地表的蒸發散量與 CV 值，以提昇流量模擬之正確性，進而結合 SEBAL 模式 (Surface Energy Balance Algorithm for Land, SEBAL)、CGCM1 大氣環流模式 (The First Version of the Canadian Global Coupled Model; CGCM1) 與 Markov 模式，模擬未來土地使用型及蒸發散量的變化，並分析其對未來流量模擬之影響，最後再綜合氣候、土地使用及蒸發散量等環境變遷因子，進一步評估台灣北部地區未來水文循環可能遭受之衝擊效應。研究方法首先利用遙測混合式分類方法進行台灣北部地區之大地資源衛星(Landsat-5)的土地使用分類，並配合數值地形模型(Digital Terrain

Model, DTM)與 SEBAL 能量平衡模式，先計算與蒸發散量有關之 16 項環境參數，再推估地表蒸發散量，並比較各土地使用型之蒸發散量，過程中為評估空間尺度和生態分類系統二因子對環境參數之影響，乃選定兩種空間尺度（台灣北部地區及其轄內的 7 個集水區）和兩種生態分類系統（12 個地理氣候分區及 7 個集水區），透過多變量逐步判別分析方法，探討該二因子對環境參數之影響效應；其次，在利用 SEBAL 模式計算蒸發散量和應用遙測方法推估 CV 值之後，進而應用 GWLF 模式模擬淡水河集水區之河川流量，目的除了驗證流量模式之適用性之外，並評估傳統查表方法和遙測方法所推估之 CV 的流量模擬差異；最後，以兩期土地使用資料為基礎，整合 Markov 模式與 CGCM1 模式，預測未來短、中、長期之土地使用變遷、並推估其 CV，再經由 GWLF 之流量分析，分析土地變遷及蒸發散變化對於未來河川流量之影響，進而評估北台灣地區水文系統可能遭遇到的衝擊效應。

研究結果指出，北台灣地區經混合式影像分類後，計分為森林、建地、水體、耕作農地、休耕農地、雲及陰影 7 類土地使用型，其整體分類準確度經檢核區檢定後為 89.00%；在土地使用型之蒸發散量方面，以森林最大（一月：0.723cm；七月：0.395cm），建地為最小（一月：0.220cm；七月：0.088cm）；在空間尺度和生態分類系統對環境參數之影響分析方面顯示，使用不同生態分類系統和空間尺度來區分 5 種土地使用型（森林、建地、水體、耕作農地及休耕農地）所需要的環境參數與參數數目皆不盡相同，但常態化差異植生指標與地表熱紅外光放射率兩項參數，不管在那一種生態分類系統，均為重要的判別參數；在利用蒸發散量和土地

使用兩因子模擬河川流量之結果顯示，利用遙測推估之 CV 值(濕季：1.245；乾季：0.851) 與查表所得之 CV 值 (濕季：0.842; 乾季：0.717) 確實有差異。若透過流量站的觀測資料，並結合迴歸分析進行模式檢核時發現，利用遙測推估值所模擬之流量與觀測流量之間的相關係數為 0.877，較查表值之 0.853 為佳；至於未來土地使用變遷與蒸發散量變化之預測結果指出，建地面積由 1995 年的 13.36%和 2002 年的 14.05%，增加為 2030 年的 38.91%，2058 年的 52.13%及 2086 年的 62.36%，此現象會造成未來短期、中期及長期之 CV 值呈逐漸下降的趨勢，而在 GWLF 模式之流量分析結果指出，不管是未來短期、中期或長期的月平均流量、年總流量及年平均流量，考慮未來土地使用變遷與蒸發散量變化兩項因子所模擬的流量均較未考慮的流量值低；最後，未來集水區水資源衝擊評估結果指出，由於都市擴張、蒸發散量減少及氣候變遷等因子之綜合作用，將造成台灣北部地區河川流量之上升。

綜合上述結果可知，整合 SEBAL、CGCM1 與 Markov 模式模擬土地使用變遷及蒸發散量變化，進而推估未來集水區之河川流量及評估區域水資源之衝擊效應，確實為一有效、可行的方法。由於台灣北部地區為經濟商業之核心區域，無論在工商業發展及水資源供給方面均占有相當重要的地位，因此相關單位應重視此課題，並及早研擬因應策略。

【關鍵詞】：遙測技術，水文循環，SEBAL 模式，GWLF 模式，CGCM1 大氣環流模式，蒸發散覆蓋係數，流量模擬。

ABSTRACT

Watershed hydrology, especially stream flow, is expected to be highly sensitive to the influences of global climate change. Traditional studies have integrated the General Circulation Models (GCMs) with the Generalized Watershed Loading Function (GWLF) model to estimate stream flow rates. However, using these models in the context of a transitioning climate and on a large spatial is problematic, particularly for the estimation of two important parameters, evapotranspiration (ET) and cover coefficient (CV).

This study focuses on an integrated analysis of the hydrological cycle using remote sensing techniques to estimate the ET and the CV. Furthermore, we improved on older studies by integrating the Surface Energy Balance Algorithm for Land (SEBAL) model, the First Version of the Canadian Global Coupled Model (CGCM1), and the Markov model which allows us to predict land-use and ET change. The results were applied to assess the future impacts of global warming on hydrological cycles of northern Taiwan. Our methods include applying hybrid image classification to generate the land-use maps of the northern Taiwan using Landsat-5 images; using digital terrain model (DTM) and the SEBAL model to calculate 16 environmental parameters relevant to ET. We then compared the differences among different land-use types; (1) investigating the effects of two ecosystem classification systems (i.e., watershed division method and geographic climate method) at various spatial scales on

environmental parameters using stepwise discriminant analysis; (2) comparing stream flow simulations according to the GWLF model with two CV values derived from remote sensing and traditional methods; (3) integrating the Markov model and the CGCM1 model to predict future land-use and CV parameters for evaluating the effect of land-use change and ET change; and (4) finally, assessing the future impacts on hydrological cycle of the northern Taiwan.

The results indicated that the study area was classified into seven land types (i.e., forest, building, water, farmland, fallow farmland, cloud-covered, and shadow-covered) with 89.09% classification accuracy. These last two land types could not be analyzed further. A comparison of daily ET values among different land-use types revealed differences. In this study, forest ET is the largest (January: 0.723cm; November: 0.395cm) while building is the smallest (January: 0.220cm; November: 0.088cm). These differences contrive to exist for ecosystem classification systems at various scales, but depend on the selected environmental parameters and the number of parameters included in the model. Two parameters, a normalized difference vegetation index and an emissivity are important factors for discriminating land types. On the aspect of land-use and ET effects on hydrological simulations, the stream flows simulated by two estimated CVs were different. The stream flow simulation using the remote sensing approach (wet season: 1.245; dry season: 0.851) presented more accurate hydrological

characteristics than the traditional approach (wet season: 0.842; dry season: 0.717). Meanwhile, according to the result of regression analysis, the flow simulation using *RSCV* (remote sensing based CV; regression coefficient = 0.877) would represent truer flow characteristics than the use of *REFCV* (reference CV; regression coefficient = 0.853). In the prediction of future land-use and ET, due to the increase of building area from 13.36% in 1995 and 14.05% in 2002 to 38.91% in 2030, 52.13% in 2052, and 62.36% in 2086, the predicated CV values for next three periods display a decreasing trend no matter under which climatic change storyline. In addition, land-use and ET change indeed affect the predicted stream flows. The predicted flows with consideration of these two factors were lower than those without consideration. Finally, the impact assessment on the hydrology of the northern Taiwan indicated that the flow volumes increase due to urban expansion, ET decline, and climate change, and it will lead to the increase of stream flow.

From above results, obviously the integration of remote sensing, the SEBAL model, the CGCM1 model, and the Markov model is a feasible scheme to predict future land-use, ET change, and stream flows. Therefore, it can be extended to the further studies in water resource management and global environmental change.

【KEYWORDS】 Remote sensing techniques, Hydrology, SEBAL model, GWLF model, CGCM1 model, Evapotranspiration cover coefficient, Stream flow simulation.

Table of Contents

口試委員會審定書.....	i
誌謝.....	ii
中文摘要.....	iii
ABSTRACT.....	iv
1. INTRODUCTION.....	1
2. MOTIVE AND OBJECTIVE.....	5
2.1.Motive.....	5
2.2.Objective.....	9
3. LITERATURE REVIEW.....	11
3.1. Land-Use Classification using Remote Sensing.....	11
3.2. Estimation of Environmental Parameters and ET based on the SEBAL Methodology.....	12
3.3. Climate Change Scenarios.....	19
3.4. Application of the GWLF Model on Hydrologic Monitoring.....	21
3.5. Prediction of Land-Use Change using Markov Model.....	27
4. STUDY AREA AND MATERIALS.....	31
4.1. Study Area.....	31
4.2. Materials.....	32
5. METHODS.....	36
5.1. Evaluation of ET Difference among Various Land-use Types.....	38

5.1.1. Classification maps of land-use using hybrid algorithm.....	38
5.1.2. Daily ET estimation based on the SEBAL model.....	39
5.1.3. Evaluation of ET difference among various land-use types.....	40
5.2. Analysis of Ecosystem Classification Systems at Various Spatial Scales on Environmental Parameters.....	40
5.3. Effect of Future Land-Use Status and ET Change for Stream Flow Simulation under Climate Change Conditions.....	43
5.3.1. Calculation of CV parameters using various methods.....	43
5.3.2. Weather generation.....	45
5.3.3. Assessment of the effects of CV on stream flow simulations.....	50
5.3.4. Predictions of land-use change and future CV values.....	50
5.3.5. Effects of land-use status and ET parameters on future stream flow simulation.....	52
5.4. Assessment of Future Impacts on Hydrological Cycle of North Taiwan.....	53
6. RESULTS.....	54
6.1. Comparison of ET Difference among Various Land-use Types.....	54
6.1.1. Land-use classification of north Taiwan.....	54
6.1.2. Estimation of the daily ET using remote sensing.....	60
6.1.3. Difference of ET among various land-use types.....	63
6.2. Effect of Ecosystem Classification Systems at Various Spatial Scales on Environmental Parameters.....	63

6.3. Assessment of Future Land-Use Status and ET Change on Stream Flow Simulation under Climate Change Conditions.....	66
6.3.1. <i>Calculations of CV under present condition</i>	66
6.3.2. <i>Validation of stream flow simulation</i>	69
6.3.3. <i>Predictions of future land-use and CV parameters</i>	75
6.3.4. <i>Effects of land-use change and ET change on future flow Simulation</i>	78
6.4. Investigation of Future Impact on Hydrological Cycle of North Taiwan.....	82
7. DISCUSSIONS.....	86
7.1. Daily ET Difference among Various Land-use Types.....	86
7.2. Estimations of Environmental Parameters under Various Ecosystem Classification Systems and Spatial Scales.....	90
7.3. Effects of Future Land-Use Status and ET Change on Stream Flow Simulation.....	91
7.4. Future Impacts on Hydrological Cycle of North Taiwan.....	93
8. CONCLUSIONS.....	94
REFERENCES.....	97

List of Tables

Table 1. Scenario parameters of the SRES-A2 experiment exported from the CGCM1 model.....	49
Table 2. Scenario parameters of the SRES-B2 experiment exported from the CGCM1 model.....	49
Table 3. A parameter comparison between traditional approach and proposed approach used in this study.....	53
Table 4. Classification of test areas.....	56
Table 5. Examination of the land-use classification of November 25, 1995.....	57
Table 6. Pixel number and percentages of five land-use types.....	60
Table 7. Computation of ET of five land-use types in 1995.....	63
Table 8. Stepwise discriminant analysis under different ecosystem classification systems at various scales.....	65
Table 9. Mean daily temperature, saturated water vapor pressure and potential evapotranspiration on July 20 and November 25, 1995.....	67
Table 10. CV obtained from remote sensing using the direct calculation procedure.....	68
Table 11. CV obtained from remote sensing using the weighted procedure.....	68
Table 12. CV obtained from the traditional approach.....	68
Table 13. Comparison between the observed and simulated temperature	

data.....	69
Table 14. Mean number of daylight hours in the study area.....	71
Table 15. Numbers of pixel and percentages of five land-use types of the Dan-Shui watershed (Excluding shadow and cloud types in both periods).....	72
Table 16. <i>RSCV</i> calculations of the Dan-Shui watershed in wet and dry seasons.....	73
Table 17. <i>REFCV</i> calculations of the Dan-Shui watershed in wet and dry seasons...	73
Table 18. Observed and simulated stream flow values (cm) of the Dan-Shui watershed.....	74
Table 19. Transitional pixels and probabilities from 1995 to 2002.....	76
Table 20. Validation of Markov prediction.....	77
Table 21. Predictions of land-use types in 2030, 2058, and 2086.....	78
Table 22. Predictions of future CV values.....	78
Table 23. Difference of stream flows (cm/month) between various approaches....	82
Table 24. Simulated flow values (cm/month) of north Taiwan under current condition.....	83
Table 25. Stream flow changes (cm) of north Taiwan due to land-use change, ET change and climate change.....	85
Table 26. CV for rice for various climatic conditions.....	89
Table 27. Evapotranspiration cover coefficients for annual crops.....	89
Table 28. Evapotranspiration cover coefficients for perennial crops.....	90

List of Figures

Figure 1. Interaction of driving forces and global environment changes.....	2
Figure 2. Illustration of the study motives.....	9
Figure 3. General computational process for determining ET using SEBAL.....	13
Figure 4. Water balance function of the GWLF model.....	22
Figure 5. The study area: the north Taiwan covered by Landsat-5 TM image.....	32
Figure 6. Location of the selected meteorological and flow stations.....	34
Figure 7. Landsat-5 TM images of the north Taiwan in three dates.....	35
Figure 8. Flowchart of the study process.....	37
Figure 9. Spatial scales and two ecosystem classification systems.....	42
Figure 10. The predicted time stages for future land-use conversions and CV values.....	51
Figure 11. Spatial distribution of the selected blocks and test areas.....	55
Figure 12. Land-use maps generated by the hybrid classification.....	59
Figure 13. Estimated energy balance parameters and ET maps of July 20, 1995.....	61
Figure 14. Estimated energy balance parameters and ET maps of November 25, 1995.....	62
Figure 15. Thiessen polygons and their influence coefficients.....	66
Figure 16. Land-use maps of the Dan-Shuei watershed from 1995.....	71
Figure 17. ET maps of the Dan-Shuei watershed from 1995.....	72

Figure 18. The observed and simulated hydrographs.....74

Figure 19. Comparison of the predicted stream flows between the traditional approach and proposed approach based on CGCM1 climate change model.....81

Figure 20. Comparison of hydrographs between current and future conditions.....84



1. INTRODUCTION

It is widely believed that an increased emission of greenhouse gases into the earth's atmosphere has likely been occurring since the industrial revolution (Arnell and Reynard 1996). From 1750 to 2000 the concentration of carbon dioxide (CO₂) and methane (CH₄) increased $31 \pm 4\%$ and $151 \pm 25\%$, respectively. Such a rapid increase not only enhances the green house effect, but also promotes the occurrence of global warming (Manning and Nobre 2001). Because of the importance of the issues, the United Nations Framework Convention on Climate Change (UNFCCC) was adopted in May 1992 and opened for signatures a month later at the United Nations Conference on Environment and Development (UNCED) in Rio de Janeiro, Brazil. The UNFCCC provides the basis for global action to protect the climate system for present and future generations. Considerable attention has been given to investigate the interactions among climate change, human activities, and nature ecosystems around the world (Figure 1).

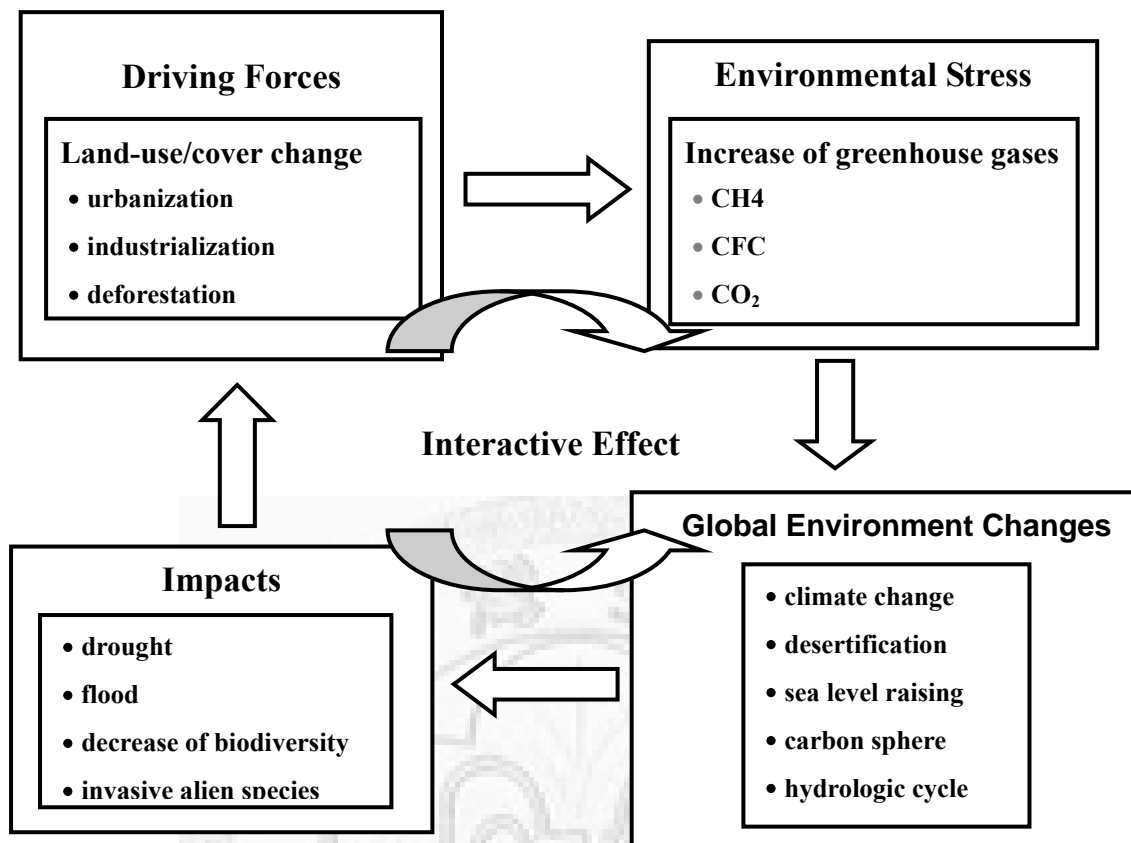


Figure 1. Interaction of driving forces and global environment changes

In the hydrologic cycle, precipitation and evapotranspiration (ET) are the main driving forces (Tung and Haith 1995), but the quantity and geographic distribution of these two factors has changed due to the increase of the average temperature of the earth. This phenomenon also affects other hydrological components such as infiltration, and stream flow, which in turn disturbs the available water resources for humans. If the current trend does not change, the impact of global warming on future climatic condition and hydrologic processes will become a major concern (Wu and Haith 1993). Estimates of global warming are usually based on the application of General Circulation

Models (GCMs), which attempt to predict the impact of increased atmospheric CO₂ concentrations on climatic variables. In order to assess the sensitivity of hydrological regimes to the climatic changes associated with global warming, previous studies have often relied on the GCMs coupled with a stream flow model, and have used these models to predict the impact of climate change on hydrologic characteristics in different areas (Yu et al. 2002). To apply these models to global environment change, the acquisition of large-scale environmental information (e.g., daily ET amount) and land-use status are necessary. ET is traditionally calculated from records of weather stations or estimated by hydrological balance functions (Chiou, 2005). These methods are limited in their ability to provide point values of ET for specific locations and fail to provide ET on a regional scale. Regarding the acquisition of land-use data, traditional ground survey methods consume much effort, money, and time. The acquisitions of multi-temporal land-use information are also problematic.

Today, remote sensing technologies have become readily available because satellite images can easily and effectively provide large scale and multi-temporal surface information for many purposes, including forest hydrology studies. The application of these newer technologies provides a more appropriate means for determining the spatial and temporal structure of ET and land-use information. If the hydrological parameters and land-use information derived from remote sensing techniques could be integrated

with an impact analysis of climate change on hydrology, it will improve the predictability of climate change effects on water resources. The combination of remote sensing, GCMs models, and stream flow models will become an important issue for hydrology study.



2. MOTIVE AND OBJECTIVE

2.1. Motive

In recent years, physically based and semi-distributed models have been frequently used to address the influence of land-use change and climate change on hydrology (Weiler et al., 2005). The Generalized Watershed Loading Functions (GWLF; Haith and Shoemaker, 1987; Haith et al., 1992; Wu and Haith, 1993) model is one of the stream flow models that incorporates the physical mechanisms and water balance relationship within a watershed. The most important advantage of using the GWLF model is that parameters can be adjusted according to the land-use types, soil characteristics and climate conditions of a watershed. For this reason, the GWLF model has been widely applied to estimate human, natural, and climate effects on hydrologic systems (Tung and Haith, 1995; Fan, 1998; Cheng et al., 2007; Markel, 2006).

In previous studies, the amount of ET in a watershed was calculated using evapotranspiration cover coefficient (CV) during the GWLF simulated procedures. The CV for each land-use type is defined as a ratio of actual ET to potential evapotranspiration (PET). However, the estimation of actual ET and CV of a large spatial scale is problematic. For example, CV can be determined from the published seasonal values based on crop types such as those given in the user's manual of the

GWLF model (Haith et al., 1992), this approach often requires estimates of crop development (e.g., planting dates, time to maturity, etc.) which may not be available. Moreover, a single set of consistent values is seldom available for all of a watershed's land-use, and settling for a cursory CV value could greatly reduce the accuracy of stream flow simulations (Haith et al., 1992, Davis and Sorensen, 1969).

The increasing availability of remote sensing technology now produces satellite images that can easily and effectively provide large scale spatial and temporal surface information. For hydrology studies, Actual ET can be computed without quantifying other complex hydrological processes through remote sensing techniques (Morse et al., 2000). Thus, much previous research adopted remotely sensed data to calculate the energy balance parameters such as surface temperature, net radiance, sensible heat flux, soil heat flux, and then estimated the actual ET according to these parameters (Chen et al., 2006; Laymon et al., 1998; Mauser and Scha'dlich, 1998; Menenti and Choudhury, 1993; Morse et al., 2000). Most of these earlier studies focused on the comparison of ET among various spatial scale and temporal stages. However, few researches have calculated CV parameters using remote-sensing-based ET for the purpose of stream flow simulation. Investigations regarding the effects of land-use types and spatial scales on ET are also seldom attempted.

In addition to the climatic factors, land-use change will influence the amount of ET,

and thereby affect the balance of the hydrologic cycle (Cheng et al., 2007). In the GWLF model, parameters such as curve number (CN) and CV are related to the land-use status of a watershed. Most previous studies assumed that catchment land-use remains consistent over long periods of time (Arnell and Reynard 1996). This assumption may reduce the accuracy of prediction. Many existing spatial simulation models have been applied in various fields (Muller and Middleton 1994; Turner 1993). A Markov model is the most widely used approach. In the Markov model, area change is summarized by a series of transition probabilities from one state to another over a specified period of time. These probabilities can be subsequently used to predict the land-use properties at specific future time points (Burham 1973). Many researchers have applied the Markov model to monitor the land-use and landscape change (Cheng et al. 2005; Lindsay and Dunn 1979; Muller and Middleton 1994; Turner 1993), but few integrate Markov predictions into hydrological assessments under changing climate conditions.

During watershed ecosystem monitoring, we observed that ecosystems are nested and reside within each other. The boundaries of ecosystems are open to transfer energy and materials to or from other ecosystems, and this linkage among systems, energy exchange to occur at various spatial scales. A disturbance to a large system may also affect smaller component systems existing within it. Consequently, the relationship

between an ecosystem at one scale and ecosystems at smaller or larger scales must be examined to predict the effects of human disturbances (Bailey, 1996, Cheng et al., 2005). Previous research has focused on the effects of global and regional scales on environmental parameters (Rao, 1990; Tokumaru and Kogan, 1993; Yu et al., 2002; Chen et al., 2006), but studies evaluate the issues of ecosystems at various scales and their effects on environmental parameters. A further investigation of the multi-scale relationship of environmental characteristics under various ecosystem classification systems is needed.

The northern part of Taiwan is a region which includes several political (ex. the capital city of Taiwan: Taipei city), scientific (ex. Hsin-chu science park), and agricultural centers (Lan-Yang flat land). These scientific or agricultural centers play important roles on technology development and crop supplies of Taiwan. An overall hydrological analysis is important in this area. Moreover, to realize how the hydrologic system would be changed in the future is also necessary for the water resource management. Figure 2 is an illustration of the study purposes.

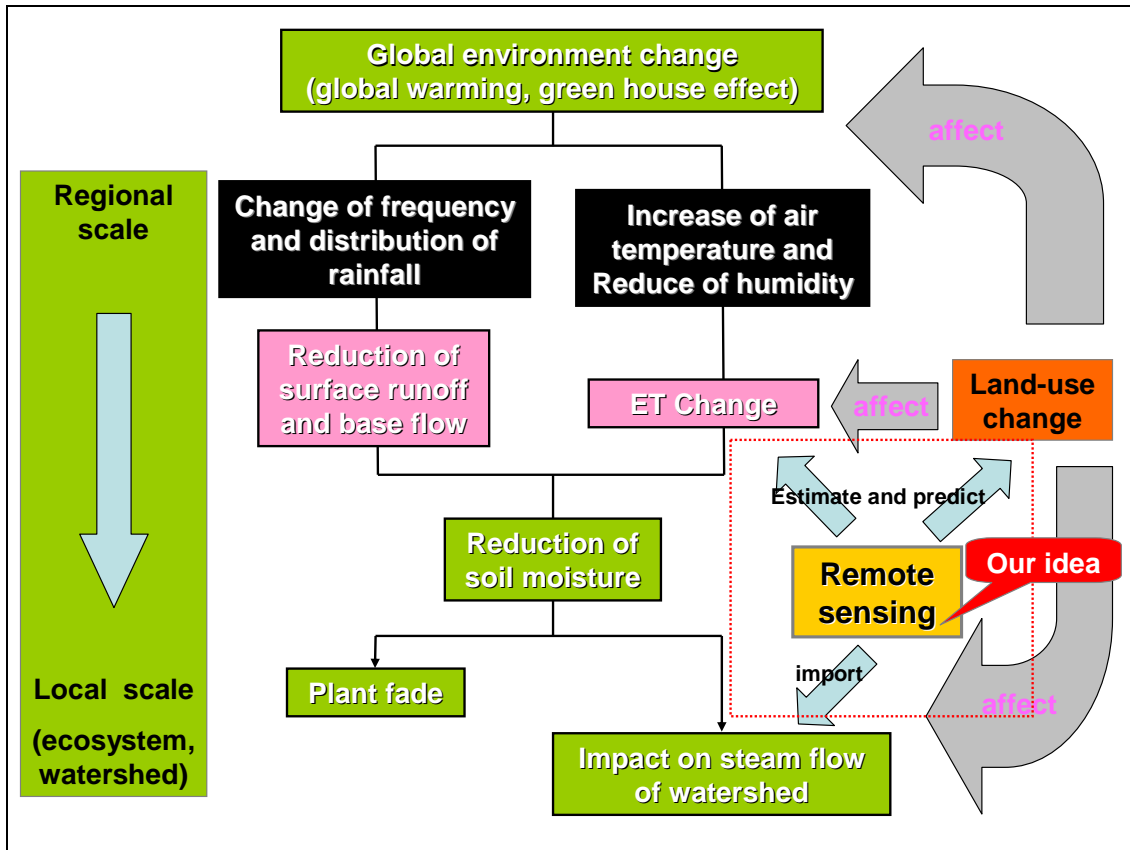


Figure 2. Illustration of the study purposes

2.2. Objective

Based on above purposes, the objectives of this study are as follows:

- (1) To evaluate the ET difference among various land-use types

Land-use maps generated by a hybrid classification approach (Hoffer and Fleming, 1978, Lo and Choi, 2004) and daily actual ET obtained from Surface Energy Balance Algorithm for Land (SEBAL; Bastiaanssen et al. 1998a) are integrated to investigate the effects of land-use types on ET.

- (2) To analyze the effect of ecosystem classification systems at various spatial scales on environmental parameters

Two spatial scales (regional scale and local) and ecosystem classification systems (geographic climate method and watershed division method) were adopted to assess their effect on environmental parameters.

(3) To investigate the effect of future land-use status and ET change on stream flow simulation under climate change conditions

Compared with the traditional stream flow simulation, which calculates a CV using the published reference values and without evaluating land-use change, our present efforts presents an approach to estimate CV by Markov model and SEBAL model, which includes future land-use status and ET change. Our study was motivated by the following three questions. Is the accuracy of stream flow simulation improved by using the CV estimated from remote sensing? Is the integration of SEBAL model and Markov model a feasible scheme to predict the future land-use and ET parameters for stream flow simulations? Does the consideration of land-use change and ET change affect the results of hydrologic assessment under climate change conditions in north Taiwan?

(4) To assess the future impact on hydrological cycle of north Taiwan

Flow series from 1995 to 2002 were adopted to represent the current hydrological condition, and then compared with the future flows to investigate how land-use change, ET change, and climate change affected river flows and the hydrologic cycle of north Taiwan.

3. LITERATURE REVIEW

3.1. Land-Use Classification using Remote Sensing

Classification of land-use and land cover using satellite images is considered an essential task in modeling the earth as a system. Traditionally, supervised and unsupervised classifications are two common image classification approaches, each with advantages and disadvantages (Lillesand and Kiefer, 2004; Lang et al., 2008). The supervised approach involves a training stage, which allows the input of analyst's experience into image classifications. However, this approach has been regarded as overly subjective and difficult to correctly implement, because user-defined training data may not be normally distributed. The unsupervised approach can automatically generate almost unlimited number of spectral classes, which are solid spectral foundations for generating information classes, but it requires the analyst manually label the resultant spectral classes into information classes (Lang et al., 2008).

To improve the accuracy of image classification, an integrated algorithm called a hybrid classification approach that takes advantage of both classification approaches has been developed (Hoffer and Fleming, 1978, Lo and Choi, 2004). In this hybrid approach, cluster analysis was first used to acquire the spectral signatures objectively, and then the signature file was imported into the supervised classification to generate the land-use

map. Hybrid classification has been widely applied in ecosystem monitoring studies, and the results from previous studies demonstrated that the integrated algorithm could provide an accurate and consistent classification of land use mapping. For example, Lo and Choi (2004) adopted the hybrid classification method to map the land use/cover of the Atlanta metropolitan area using Landsat 7 Enhanced Thematic Mapper Plus (ETMz) data; Lang et al. (2008) applied the hybrid approach to generate a land-use map of Indiana, USA. Lillesand and Kiefer (2004) indicated that the hybrid approach indeed increased the repeatability and accuracy of land-use classification.

3.2. Estimation of Environmental Parameters and ET based on the SEBAL Methodology

SEBAL is an image processing model that calculates the actual ET and other energy exchanges at the earth's surface using digital image data collected by Landsat or other remote sensing satellites measuring visible, near infrared, and thermal infrared radiation (Bastiaanssen et al., 1998a). The major concept of this model is that ET flux is calculated as a residual of the surface energy budget equation and is expressed as the energy consumed by the evaporation process:

$$LE = Rn - G_0 - H \quad (1)$$

where, LE is the latent heat flux (W/m^2); Rn is the net radiation flux at the surface (W/m^2); G_0 is the soil heat flux (W/m^2); H is the sensible heat flux to the air (W/m^2). LE is converted into ET, expressed as a depth of water per time, by dividing by the latent heat of vaporization.

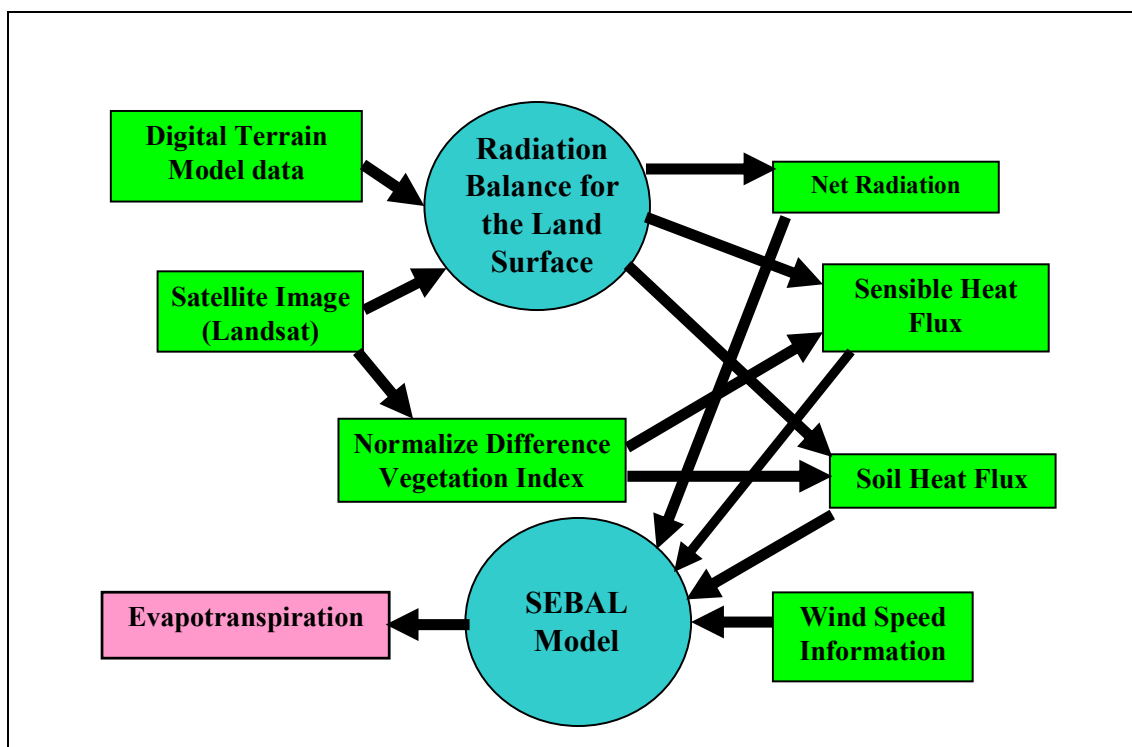


Figure 3. General computational process for determining ET using SEBAL

(Morse et al., 2000)

Figure 3 is the schematic of the general computational process for determining ET using SEBAL. During the model processes, actual ET is computed as a component using 15 energy balance parameters, including the cosine of solar incidence angle ($\cos\theta$;

unitless), twenty-four hour extraterrestrial radiation (Ra_{24} ; W/m^2), surface albedo at the top of atmosphere (α_{toa} ; unitless), surface albedo (α_0 ; unitless), normalized difference vegetation index ($NDVI$; unitless), emissivity (ε_0 ; unitless), surface temperature (T_0 ; K), transmittance (τ_{sw} ; unitless), air density (p_{air} ; kg/m^3), aerodynamic resistance to heat transport (r_{ah} ; s/m), estimating friction velocity (u^* ; m/s), surface roughness for momentum transport, (z_{om} ; m), net radiation (Rn ; W/m^2), soil heat flux (G_0 ; W/m^2), sensible heat flux (H ; W/m^2) (Morse et al., 2000). In SEBAL procedures, R_n was estimated based on the following relationship (Bastiaanssen et al., 1998; Oberg and Melesse, 2004):

$$R_n = R_{s\downarrow}(1 - \alpha) + R_{L\downarrow} - R_{L\uparrow} - R_{L\downarrow}(1 - \varepsilon_0) \quad (2)$$

where, $R_{s\downarrow}$ is the incoming direct and diffuse shortwave solar radiation that reaches the surface (W/m^2); α is the surface albedo, the ratio of reflected radiation to the incident shortwave radiation; $R_{L\downarrow}$ is the incoming longwave thermal radiation flux from the atmosphere (W/m^2); $R_{L\uparrow}$ is the outgoing longwave thermal radiation flux emitted from the surface to the atmosphere (W/m^2); ε_0 is the surface emissivity, the ratio of the radiant emittance from a gray body to the emittance of a blackbody.

Soil heat flux (G_0) is the rate of heat storage to the ground from conduction. In the

SEBAL model, an empirical relationship for G_0 was given as:

$$G_0 = 0.30(1 - 0.98NDVI^4)R_n \quad (3)$$

where, $NDVI$ is the normalized difference vegetation index.

Sensible heat flux (H) is the rate of heat loss to the air by convection and conduction due to a temperature difference. The calculated equation was as bellow:

$$H = \frac{\rho C_p dT}{r_{ah}} \quad (4)$$

where, ρ is the density of air (kg/m^3); c_p is the specific heat of air (1004 J/kg/K); dT is the difference in temperature between the surface and the air (K); and r_{ah} is the aerodynamic resistance (s/m). To calculate dT , the inverse of equation (5) was considered:

$$dT = \frac{H \times r_{ah}}{\rho C_p} \quad (5)$$

Therefore, during the SEBAL process, the user calculated dT at two extreme

“anchor pixels” by assuming values for H at the reference pixels. The reference pixels were carefully chosen so that at these pixels one can assume that H approximate zero at a very wet pixel (i.e., all available energy ($R_n - G_0$) is converted to ET), and that LE almost equals zero at a very dry pixel, so that $H = R_n - G_0$. These assumptions from the selected pixels provided endpoints for values and locations for H so that a relationship for dT can be established.

Once the values of H and G_0 were calculated, the latent heat flux (LE) can be calculated from equation (1). This LE represented the instantaneous evapotranspiration at the time of the Landsat overpass. Following the computation of the evaporative fraction at each pixel of the image, one can estimate the 24-hour evapotranspiration for the day of the image by assuming that the value for the evaporative fraction () is constant over the full 24-hour period (Bastiaanssen et al. 1998). The evaporative fraction is calculated for the instantaneous values in the image as:

$$\hat{\epsilon} = \frac{R_n - G_0 - H}{R_n - G_0} \quad (6)$$

where, the values for R_n , G_0 , and H are instantaneous values taken from processed images. The 24 hour actual evaporation is calculated by the following equation:

$$ET_{24} = \frac{86400 \wedge (R_{n24} - G_{24})}{\lambda} \quad (7)$$

where, ET_{24} is daily actual evapotranspiration (cm/day); R_{n24} is daily net radiation; G_{24} is daily soil heat flux; 86,400 is the number of seconds in a twenty-four hour period; and λ is the latent heat of vaporization (J/kg). The latent heat of vaporization allows expression of ET_{24} in cm/day.

Many previous studies applied remotely sensed data to calculate the energy balance parameters, and then estimated the actual ET according to these parameters. For example, Chen et al. (2006) applied the SEBAL model and four seasons of moderate resolution imaging spectroradiometer (MODIS) satellite images to estimate ET for the entire island of Taiwan; Laymon et al. (1998) used Landsat thematic mapper (TM) images and experience functions to estimate energy fluxes and latent heat flux, and further to calculate the ET in a semidesert area of West America; Mauser and Scha'dlich (1998) modeled the spatial distribution of ET on a different scale using remote sensing data; Menenti and Choudhury (1993) applied Landsat MSS data to develop the surface energy balance index (SEBI) model, and then to estimate the ET of the Libyan desert in West Africa by using surface albedo and aerodynamic roughness; Morse et al. (2000) applied the SEBAL model and satellite images to calculate the ET, and the results showed that the R^2 value between ET acquired from remote sensing and observed data

was 0.98.

Physical parameters obtained from the SEBAL model also have special meanings on the description of temperature, vegetated, hydrological and energy characteristics of an ecosystem. For example, Ra_{24} is the daily incoming solar radiation unadjusted for atmospheric transmittance; α_{toa} and α_0 indicate the ratio of reflected to incident solar radiation at the atmosphere and ground surface; ε_0 and T_0 are temperature indices which denote the thermal energy radiated by the surface and surface temperature conditions of the area; $NDVI$ is a sensitive indicator of the amount and condition of green vegetation; z_{om} is defined as the height above the “zero-plane displacement” that the zero-origin for the wind profile just begins within the surface or vegetation cover; Rn is the net radiant energy that the land surface actually receives and loses from or to the atmosphere. The allotment of Rn represents the energy transmission process within the ecosystem. Rn is divided into three components; ET_{24} is the twenty-four hour actual evapotranspiration. It also indicates the energy that used to support the photosynthesis and evaporate soil water; H is the energy used to heat the air; G_o is the rest of the net energy which is stored in the ground or water body. The above environmental parameters were computed by the SEBAL model based on an energy balance algorithm. However, the acquisition of surface reflectance would vary with different terrains and meteorological conditions. For instance, the instantaneous and 24-hour solar radiations on a south slope

are much higher than on a north slope in the Northern Hemisphere. Atmospheric humidity and soil moisture are two important factors for ground reflectance, and they might influence the calculation of environmental parameters (Cheng et al., 2008).

3.3. Climate Change Scenarios

Climate change is a very complex issue. Policymakers need an objective source of information about the causes of climate change, its potential environmental and socio-economic consequences, and the adaptation and mitigation options to respond to it. This is why World Meteorological Organization (WMO) and UNEP established the Intergovernmental Panel on Climate Change (IPCC) in 1988.

The IPCC is a scientific body. The information it provides with its reports is based on scientific evidence and reflects existing viewpoints within the scientific community. The comprehensiveness of the scientific content is achieved through contributions from experts in all regions of the world and all relevant disciplines including, where appropriately documented, industry literature and traditional practices, and a two stage review process by experts and governments.

The IPCC currently has three Working Groups and the Task Force on National Greenhouse Gas Inventories. The Working Groups and the Task Force have clearly defined mandates as agreed by the Panel and their activities are guided by two Co-chairs

each. They are assisted by a Technical Support Unit and the Working Group or Task Force Bureau. Working Group I (WG I) deals with "The Physical Science Basis of Climate Change", Working Group II (WG II) with "Climate Change Impact, Adaptation and Vulnerability" and Working Group III (WG III) with "Mitigation of Climate Change". The main objective of the Task Force is to develop and refine a methodology for the calculation and reporting of national green house gas emissions and removals. In addition to the Working Groups and Task Force, further Task Groups and Steering Groups may be established for a limited or longer duration to consider a specific topic or question (IPCC, 2004).

At regular intervals, the IPCC provides assessment reports of the state of knowledge on climate change, which become standard works of reference, widely used by policymakers, experts, and students. The findings of the first IPCC Assessment Report of 1990 played a decisive role in leading to the United Nations Framework Convention on Climate Change (UNFCCC), which was opened for signature at the Rio de Janeiro Summit in 1992 and enacted in 1994. It provides the overall policy framework for addressing the climate change issue. The IPCC Second Assessment Report of 1995 provided key input for the negotiations of the Kyoto Protocol in 1997, and the Third Assessment Report of 2001, as well as Special and Methodology Reports, provided further information relevant for the development of the UNFCCC and the

Kyoto Protocol. The IPCC continues to be a major source of information for the negotiations under the UNFCCC. The latest one is "Climate Change 2007", the Fourth IPCC Assessment Report (IPCC, 2007).

In 2000 the IPCC published a new set of emission scenarios, which address changes in the understanding of driving forces and emissions and methodologies since the completion of the IPCC IS92 scenarios. The Special Report on Emissions Scenarios (SRES) are based on an extensive assessment of driving forces and emissions in the literature, alternative modeling approaches and an "open process" that solicited participation and feedback from scientist's around the world. An important part of this report is the consideration of the contributions to future emissions, from demographic to technological and economic developments, but, as requested in the terms of reference, none of the scenarios included future policies that explicitly address climate change. Four different storylines were developed to describe the relationship between emission driving forces, and their evolutions, and add context to the scenario quantification (IPCC, 2000).

3.4. Application of the GWLF Model on Hydrologic Monitoring

The GWLF model is a physical hydrological model, which simulates the water balance within an upstream watershed. In the GWLF model, the stream flow consists of

runoff and discharge from groundwater. The latter is obtained from a lumped parameter watershed water balance. Daily water balance is calculated for unsaturated and shallow saturated zones. Infiltration to the unsaturated and shallow saturated zones equals the excess, if any, of rainfall and snowmelt less runoff and ET. Percolation occurs when unsaturated zone water exceed field capacity. The shallow saturated zone is modeled as a linear groundwater reservoir (Haith et al., 1992). The model structure of GWLF is shown as Figure 4.

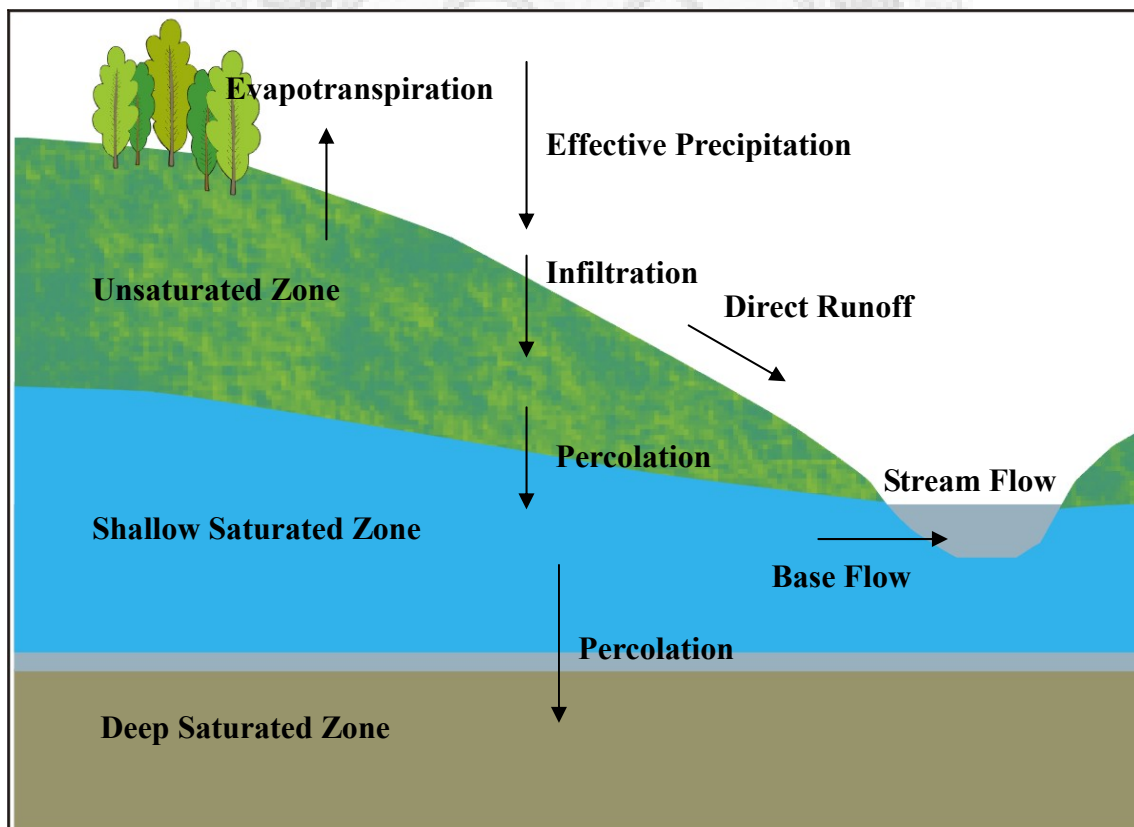


Figure 4. Water balance function of the GWLF model

(modified from Haith et al., 1992)

$$SF_t = G_t + Q_t \quad (8)$$

where, SF_t is the stream flows of a watershed (cm); G_t is the groundwater discharge (cm); Q_t is the surface runoff (cm).

Groundwater discharge is estimated by assuming shallow saturated zone as a linear reservoir using the follow equation:

$$G_t = r \times S_t \quad (9)$$

where, r is the recession coefficient; S_t is the storage of shallow saturated zone (cm).

To estimate surface runoff, the GWLF model used the curve number method to calculate runoff volumes with the considerations of land-use status and antecedent soil moisture. The equations are as follows:

$$Q_t = \frac{(R_t - 0.2W_t)^2}{(R_t + 0.8W_t)} \quad (10)$$

$$W_t = \frac{2540}{CN_t} - 25.4 \quad CN \leq 100 \quad (11)$$

where, Q_t is the surface runoff (cm); R_t is the daily precipitation (cm); CN is the curve number; W_t is the maximum soil runoff load (cm).

Curve number is selected as functions of land use types, soil texture and antecedent moisture. Curve number for antecedent moisture conditions 1 (driest), 2 (average) and 3 (wettest) are $CN1$, $CN2$, and $CN3$, respectively. $CN2$ can be determined by referring to the GWLF manual, and $CN1$ and $CN3$ can be calculated from $CN2$. The functions of $CN1$ and $CN3$ are as follows (Haith et al., 1992):

$$\begin{aligned}
 CN1 &= \frac{CN2}{2.334 - 0.01334CN2} \\
 CN3 &= \frac{CN2}{0.4036 + 0.0059CN2}
 \end{aligned}
 \tag{12}$$

Moisture leaves the ground surface of a watershed as ET, that is, transpiration by plants and evaporation from moist soil and the stream surface (Weisman, 1977). Estimation of ET for watershed studies is problematic (Haith et al. 1992). In the GWLF model, ET is estimated as a function of the atmospheric and surface characteristics of a watershed, as equation (8).

$$ET_t = CV \times PET_t \quad (13)$$

where, ET_t is evapotranspiration (cm); CV is cover coefficient; PET_t is potential evapotranspiration (cm) as given by Hamon (1961):

$$PET_t = \frac{0.021H_t^2 e_{0t}}{T_t + 273} \quad (14)$$

where H_t is the number of daylight hours per day during the month containing day t ; e_{0t} is the saturated water vapor pressure in millibars on day t , and T_t is the temperature on day t ($^{\circ}\text{C}$). Saturated water vapor pressure can be approximated as in Bosen (1960):

$$e_{0t} = 33.8639[(0.00738 \times T_t + 0.8072)0.8 - 0.000019 \times |1.8 \times T_t + 4.8| + 0.00136] \quad (15)$$

In urban areas, ground cover is a mixture of trees, grass, water, and concrete constructions. It follows that CV for an area are weighted averages of the perennial crop, hardwood and softwood forest, water, and construction factors, as equation (16) and (17).

$$cv_i = \frac{ET_i}{PET_i} \quad (16)$$

$$CV_e = \sum_{i=1}^m cv_i \times w_i \quad (17)$$

where, cv_i is CV of class i ; ET_i is ET of class i (mm/day); CV_e is the CV for the entire area; w_i is percentage of class i ; PET_i is potential evapotranspiration (cm).

Stream flows calculated by the GWLF model are based on a consideration of water balance within a watershed. Compared with other models, the GWLF model uses fewer parameters but processes a high degree of predictive accuracy. Consequently, many studies (Haith et al., 1992; Tung et al., 1999; Yu et al., 2002; Markel et al., 2006) applied the GWLF model to assess the watershed hydrology and stream flow volume, and also to validate the flow prediction of the GWLF model. For example, Haith et al. (1992) tested the GWLF model by comparing model predictions with measured stream flow from the West Branch Delaware River Basin (area = 850 km²) during a three-year period. The result showed that the derived coefficient of determination (R^2) is 0.88, indicating that the model explains at least 88% of the observed monthly variation in stream flow. Although better results could perhaps be obtained by more detailed hydrologic models, such models have substantially greater data and computational requirements and must be calibrated from sampling data.

Many previous studies often rely on the GCMs coupled with the GWLF model to assess the sensitivity of hydrological regimes to the climatic changes associated with global warming (Yu et al. 2002). For example, Tung and Haith (1995) used the GWLF model and two kinds of GCMs scenarios to assess the impacts of global warming on stream flows for four large watersheds in New York State. Fan (1998) developed a procedure to evaluate the impacts of climate change on ground water recharge in Taiwan using the GWLF model and four climate change scenarios. Cheng et al. (2007) integrated the Markov model and the SRES scenario to investigate the influence of future land-use changes and climate changes on the stream flow simulations using the GWLF model, and also to assess the impacts on the Jiao-Long watershed of central Taiwan.

3.5. Prediction of Land-Use Change using Markov Model

The Markov model is a stochastic model. During its process, land-use change of an area is summarized by a series of transition probabilities from one state to another over a specified period (Hillier and Lieberman, 1995). These probabilities can be subsequently used to project the landscape properties at alternate future time points (Burham, 1973).

The Markov model assumes that the land-use changes of the study area could be

depicted as a Markov process. A transition matrix, in which the element T_{ij} represents the amount of land-use change from type i to type j during two periods, are derived from the land-use maps (Cheng, et al., 2006). The transition probability P_{ij} , which represents the fractions of land-use changes on each land-use type, is estimated by:

$$P_{ij} = T_{ij} / \sum_{j=1}^m T_{ij} ; i = 1, 2, \dots, m, \quad (18)$$

where, m is the number of land-use types.

To determine whether it is appropriate to apply the Markov model to the observed land-use changes, Goodman's Chi-squared statistic (Goodman 1968) was used to test the null hypothesis that the land-use conditions in 1995 and 2002 were independent of each other. If the calculated χ^2 is larger than the reference value, we reject the hypothesis that land-use change during the period is a random procedure. In other word, the transition process is a Markov chain procedure. We can apply the Markov model to predict the possible land-use change of the area.

$$\chi^2 = \left\{ \sum_{i=1}^m \sum_{j=1}^m [T_{ij} \times \ln(P_{ij} / A_j)] \right\}^2 ; df = (m-1)^2 \quad (19)$$

where, the definitions of T_{ij} and P_{ij} are same as in equation (18), A_j is the fraction of land-use in each of the land-use types in 1995; df is the degree of freedom.

Assuming that the transition probabilities will remain constant in the future, the Markov model is then used to project the land-use at the next stage:

$$n_{t_2} = P \cdot n_{t_1} \quad (20)$$

where, P is the transition probability matrix, n_{t_1} and n_{t_2} are column vectors denoting the fractions of land-use types at t_1 and t_2 .

The Markov model is a widely used approach to evaluate the change of land-use types, landscape distribution, and ecosystem environment (Wu, 2004). For example, Turner (1993) used the Markov transition probability to monitor the landscape changes in nine rural counties in Georgia, USA; Avaiksoo (1995) simulated the vegetation dynamics and land use in a mire landscape using a Markov model; Hsu and Cheng (2000) assessed the landscape change in Liukuei ecosystem area using a Markov model. Lindsay and Dunn (1979) applied a transition matrix approach to project the land use status under alternative policies; Muller and Middleton (1994) used a Markov model to

simulate the land-use change dynamics in the Niagara Region, Ontario, Canada.

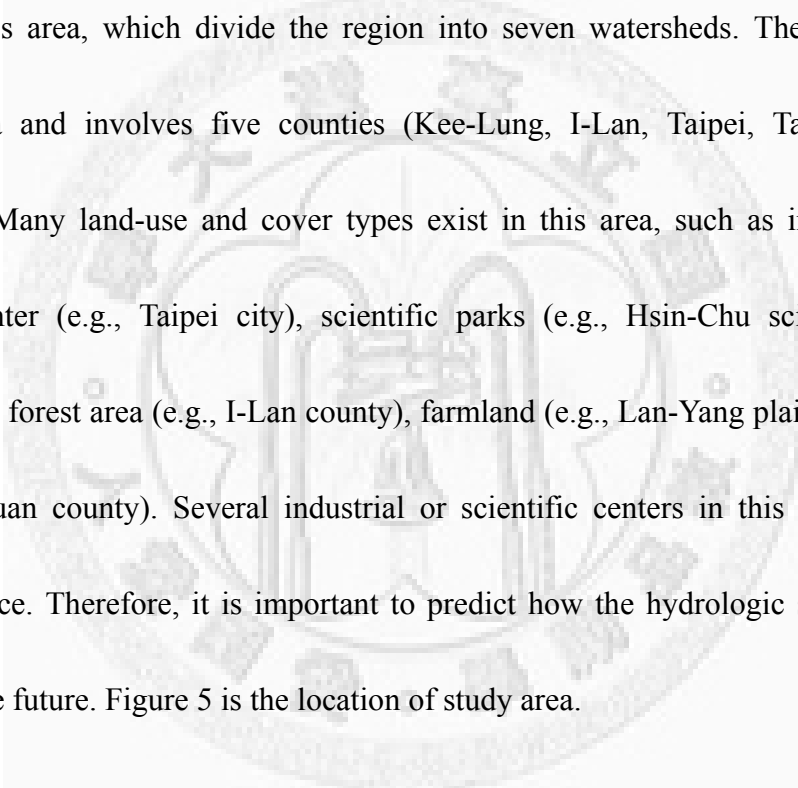
This present study will contribute to these past efforts by proposing a hybrid of SEBAL, GCMs, and GWLF models in order to simulate more accurate hydrological change based on climate change conditions.



4. STUDY AREA and MATERIALS

4.1. Study Area

The study area selected for the empirical analysis was the north of Taiwan. There are four main streams (Dan-Shui river, Kee-Lung river, Xin-Dian river, and Da-Han creek) in this area, which divide the region into seven watersheds. The area covers 734589.7 ha and involves five counties (Kee-Lung, I-Lan, Taipei, Tao-Yuan, and Hsin-Chu). Many land-use and cover types exist in this area, such as industrial and business center (e.g., Taipei city), scientific parks (e.g., Hsin-Chu science parks), mountainous forest area (e.g., I-Lan county), farmland (e.g., Lan-Yang plain) and ponds (e.g., Tao-Yuan county). Several industrial or scientific centers in this area demand water resource. Therefore, it is important to predict how the hydrologic system could change in the future. Figure 5 is the location of study area.



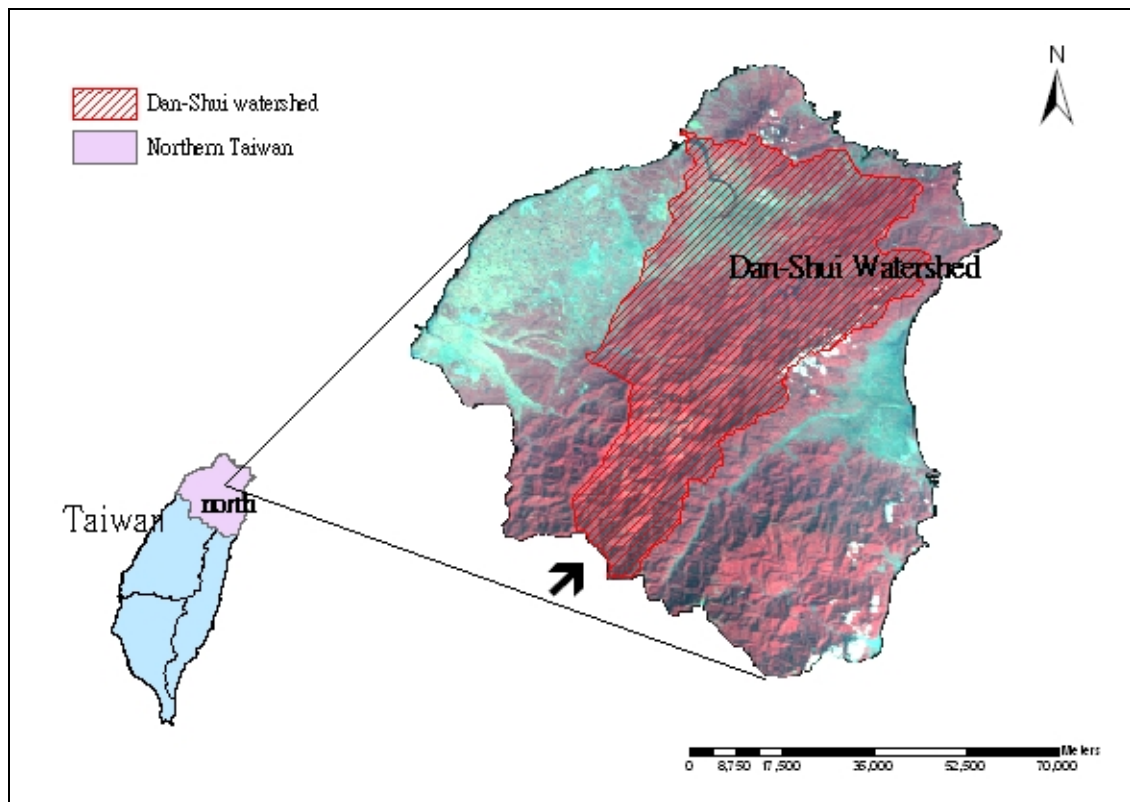


Figure 5. The study area: the north Taiwan covered by Landsat-5 TM image

4.2. Materials

Five kinds of data were consulted for this study, Landsat-5 TM images of 1995 and 2002, digital terrain model (DTM), national land-use inventory data in 1995, and daily observational records of weather and stream flow. First, three Landsat-5 TM images from different dates (July 20 and November 25, 1995; January 4, 2002) were adopted. Landsat-5 TM images contain seven spectral bands ranging from the visible blue to the middle infrared (mid-IR). Bands 1 to 3 are the blue, green, and red bands; band 4 is the

near IR; band 5 and band 7 are the mid-IR. Each of above six bands has a 30 m ground resolution. Band 6 is the thermal IR with 120 m resolution. The extent of the study area was clipped from the raw images and used to generate land-use maps. Second, DTM with 40 m resolution was provided by the aerial survey office, Forestry Bureau. The DTM data was used to derive the slope, aspect, and elevation information for modification of the SEBAL model in a mountainous area. National land-use inventory data generated in 1995 by the Department of Land Administration, the Ministry of the Interior is regarded as the paragon for evaluating image classification. The period from 1995 to 2002 was selected as the baseline, representing “current climatic conditions”. Daily temperature and precipitation data were collected from seven meteorological stations. These are: Fu-Guei-Jiao, Cyu-Chih, Sin-Wu, Cyue-Ci, Mei-Hua, Yi-Lan and Sih-Yuan weather stations. The Dan-Shui watershed, which occupies the largest drainage area in north Taiwan, was assigned to be the sample for model validation. Climatic records at the Cyu-Chih meteorological station and stream flow observations at Shang-Guei-Shan-Ciao flow station were collected from 1995 to 2002. Although the distance between two gauged stations is less than 1 km, both stations have similar elevation (Cyu-Chih station: 90.0m; Shang-Guei-Shan-Ciao station: 70.9m). Thus the meteorological stream flow data collected from these two stations is comparable for hydrological analysis. Figure 6 shows the location of the selected meteorological and

flow stations. Figure 7 shows the Landsat-5 TM images used in this study.

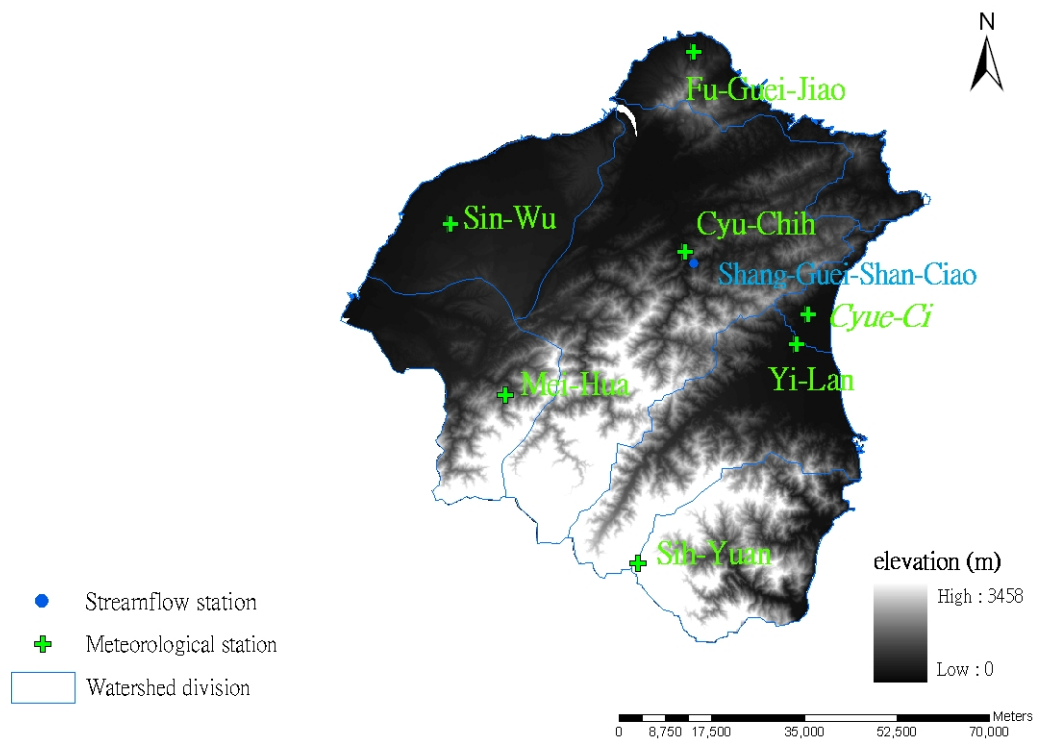


Figure 6. Location of the selected meteorological and flow stations

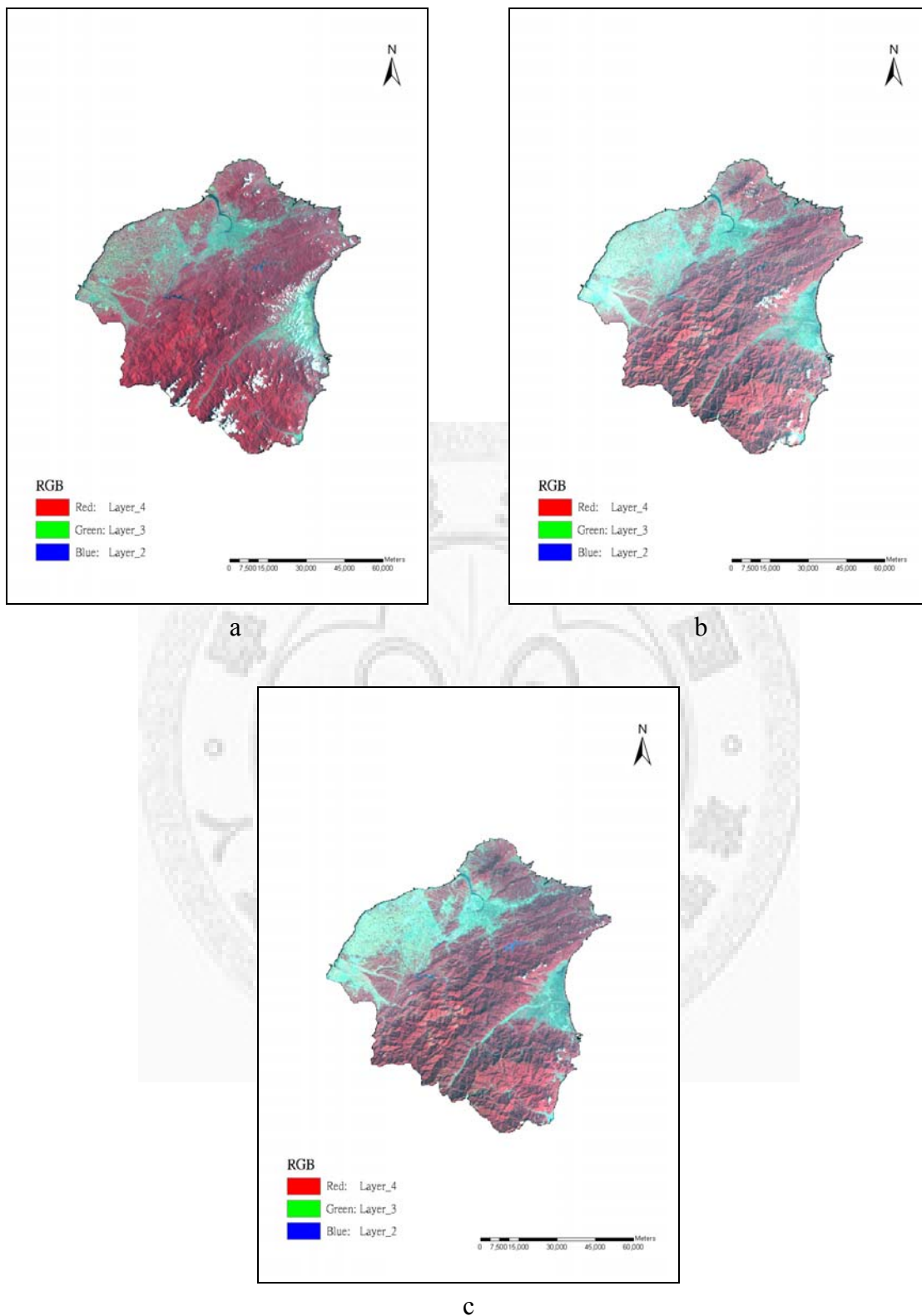
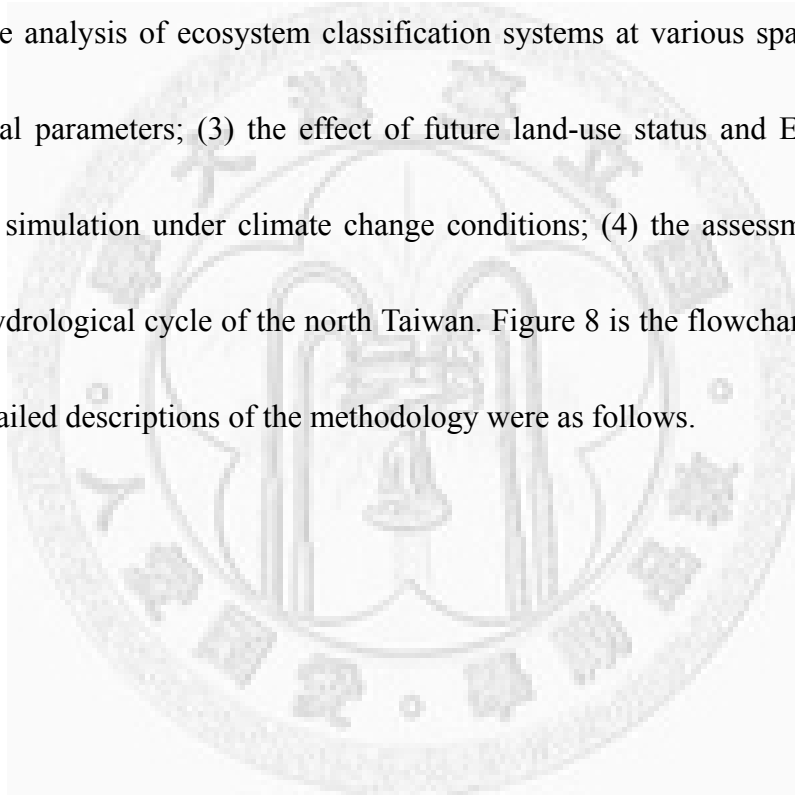


Figure 7. Landsat-5 TM images of the north Taiwan in three dates

(a: July 20, 1995; b: November 25, 1995; c: January 4, 2002)

5. METHODS

This study integrated the SEBAL model, the CGCM1 model, and the Markov model to monitor the hydrological cycle of the north Taiwan through remote sensing. The processes included: (1) the evaluation of ET difference among various land-use types; (2) the analysis of ecosystem classification systems at various spatial scales on environmental parameters; (3) the effect of future land-use status and ET change for stream flow simulation under climate change conditions; (4) the assessment of future impact on hydrological cycle of the north Taiwan. Figure 8 is the flowchart of the study process. Detailed descriptions of the methodology were as follows.



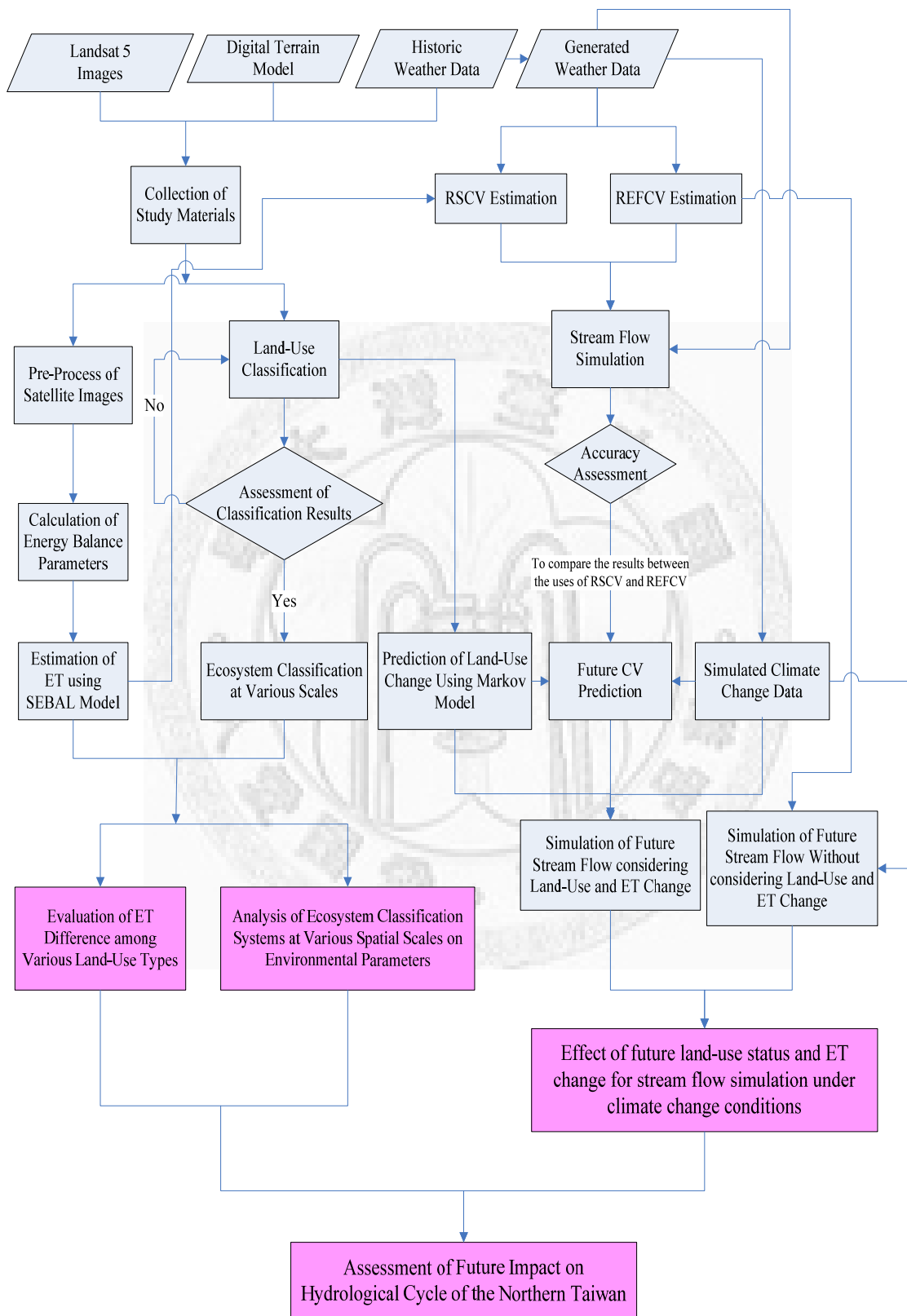


Figure 8. Flowchart of the study process

5.1 Evaluation of ET Difference among Various Land-use Types

5.1.1. Classification maps of land-use using hybrid algorithm

Hybrid classification is an integrated algorithm which combines the advantages from both traditional supervised and unsupervised approaches (Hoffer and Fleming 1978, Lo and Choi 2004). In this hybrid approach, cluster analysis was first used to acquire the spectral signatures objectively, and then the signature file was imported into the supervised classification to generate the land-use map. The analytical procedures included four steps: (1) Eight blocks were first selected from the study image according to ground land-use information. Each block contained three to four kinds of land-use types; (2) In the unsupervised stage, the selected blocks were clustered into spectral subclasses by unsupervised classification and then merged or deleted subclass signatures as appropriate based on transformed divergence (TD), see equation 21. TD ranged from 0 to 2000. If two classes can be separated completely, then the TD approaches 2000; (3) Spectral signatures obtained from each block were then combined and integrated into a single spectral signature; Finally (4) in the supervised stage: the single spectral signature was finally applied to generate the land-use map of the study area.

$$TD = 2000 [1 - \exp(-D/8)]$$

$$D = \frac{1}{2} \text{tr} (Cov_i Cov_j) Cov_i^{-1} - Cov_i^{-1} + \frac{1}{2} \text{tr} [Cov_i^{-1} - Cov_j^{-1} (m_i - m_j)(m_i - m_j)^T] \quad (21)$$

where, TD is the transformed divergence (-); D is the divergence; Cov_i is the covariance matrix of class i ; m is the mean vector of class i ; and $\text{tr}[A]$ is the sum of the diagonal line of matrix A .

To evaluate the result of land-use classification, test areas for each cover type were selected from the generated map of November 25, 1995. All test areas were used to compare with the national land-use inventory data, and the classification accuracy was then calculated. The same procedures were adopted to generate the land-use maps of July 20, 1995 and January 4, 2002.

5.1.2. Daily actual ET estimation based on the SEBAL model

The SEBAL model was used to compute 15 energy balance parameters, and then to calculate actual ET according to these parameters. Moreover, in order to consider the seasonal changes of ET, two actual ET maps (July, 20 and November, 25, 1995) were calculated. Mean daily ET values derived from the two ET maps were applied to define the actual ET amount and CV parameters for various land-use types in further steps.

5.1.3. Evaluation of ET difference among various land-use types

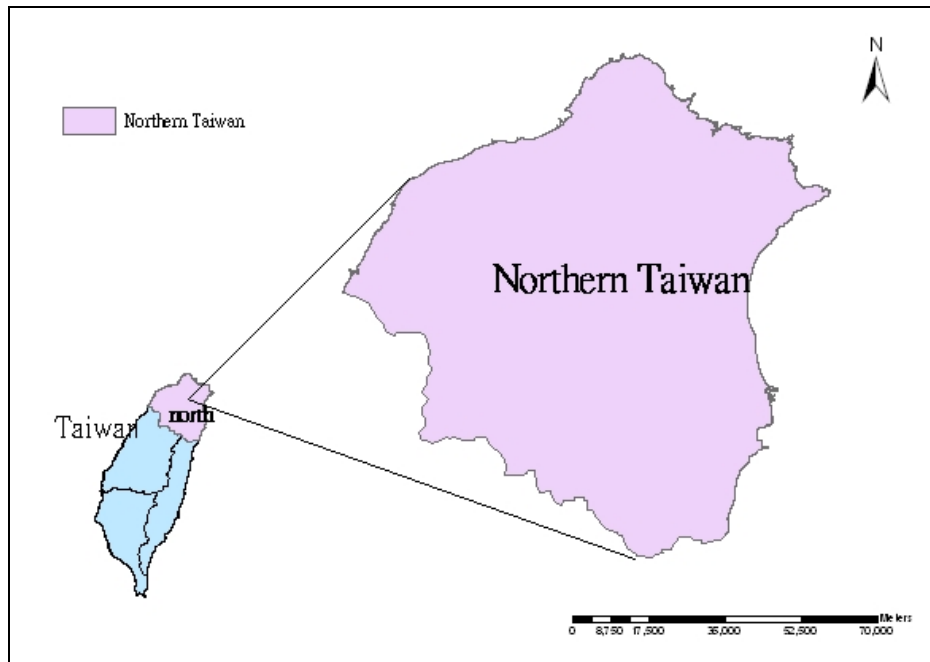
Land-use maps generated using the hybrid approach and daily ET obtained from the SEBAL model were used to compare the difference among various land-use types in different seasons. However, because even a thin layer of shadow or cloud can considerably obscure the thermal band readings and cause large errors in calculation of ET (Morse et al., 2000), two cover types (i.e., shadow and cloud) within the study site were eliminated prior to the comparison.

5.2. Analysis of Ecosystem Classification Systems at Various Spatial Scales on Environmental Parameters

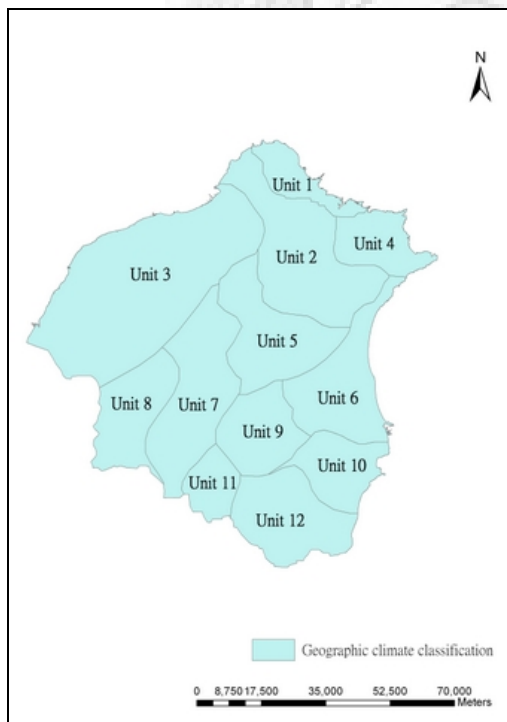
To assess the effect of ecosystem classification systems at various scales on environmental parameters, two methods of ecosystem classification were used in this study. One is called the geographic climate method which is based on the controlling factors such as temperature and precipitation to classify land as ecosystems (Su, 1992). The other is called the watershed division method which is based on the DTM to automatically extract watershed and regards watershed units as ecosystems. Under various scales of ecosystem classification systems (regional and local scales), the study area was further classified into different numbers of ecosystem units, for example, geographic climate method and watershed division method have 12 and 7 ecosystem

units, respectively (Figure 9). Ecosystem units obviously have unique characteristics of climate or terrain no matter what the ecosystem classification. For example, the major climate type in unit 3 of the geographic climate method is summer rain climate, and unit 6 is everwet climate. But for the watershed division method, unit 3 was identified as a flat plain, and unit 2 is in a steep mountainous area. In addition, there are several industrial and scientific campuses in the study area, which demand more water resources and may indirectly influence the operation of ecosystem. Therefore, it is important to understand how land-use types and ecosystem classification systems affect the environmental parameters before making management decisions.

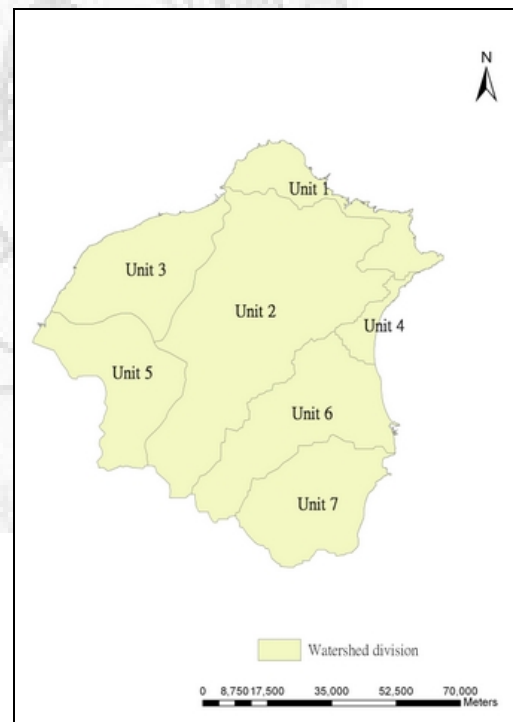
During the process, land-use types were regarded as the dependent variables and 16 environmental parameters (15 energy balance parameters + actual ET) obtained from the SEBAL model were regarded as the independent variables. Stepwise discriminant analysis was used to select the optimal combination of parameters for discriminating five land-use types, and further to assess the effect of ecosystem classification systems at various scales on environmental parameters. Wilks' lambda was used to determine which independent variables contributed to the discriminant function significantly. The Wilks' lambda ranges from zero to one, with 0 indicating groups are different and one meaning groups are the same.



a



b



c

Figure 9. Spatial scales and two ecosystem classification systems

(a: regional scale: the north Taiwan; b: local scale: geographic climate method; c: local scale: watershed division method)

5.3. Effect of Future Land-Use Status and ET Change for Stream Flow

Simulation under Climate Change Conditions

5.3.1. Calculation of CV parameters using various methods

This study used two various methods to estimate CV parameters. The first method, an innovation in the study, was to calculate the CV using remote sensing techniques (i.e., *RSCV*). Two different procedures could be applied to derive the CV using satellite data. The first one was a direct calculation procedure, which combined the water balance function used in the GWLF model and actual ET obtained from Landsat-5 TM images, and then to compute the remote sensing based CV for the entire study site directly (called the *RSCV_d*). Due to the seasonal changes of vegetation structure and growing status, the values of CV should show seasonality. The assumption was made that May to October was the wet season and November to April was the dry season when calculating the CV, as suggested by Tien (2003) and Haith et al. (1992). Therefore, cover coefficients estimated from the actual ET of July 20, 1995 and November 25, 1995 represented the wet and dry season's CV values, respectively. The following were the equations for calculating *RSCV_d*.

$$\begin{aligned} ET_{rs} &= RSCV \times PET_t \\ RSCV_d &= \frac{ET_{rs}}{PET_t} \end{aligned} \quad (22)$$

where, ET_{rs} is the daily evapotranspiration (cm/day) of the overall study site by using remote sensing; $RSCV_d$ is the overall cover coefficient derived from remote sensing using direct calculation procedure.

The second method of estimating the CV using the remote sensing images was a weighted calculation procedure. It integrated the results of land-use classification with the actual ET obtained from SEBAL model, and then computed a CV for each land-use type. To estimate the overall CV for the study area, the percentage of land-use types was regarded as a weighting factor. The CV obtained from the weighted procedure was called the $RSCV_w$. The advantage of this method is future CV values could be obtained from the function of land-use status and PET under the assumption that the ET of land-use types was invariable in the future. The calculation equations of $RSCV_w$ were as equation (23) and (24).

$$cvrs_i = \frac{ET_i}{PET_i} \quad (23)$$

$$RSCV_w = \sum_{i=1}^m cvrs_i \times w_i \quad (24)$$

where, $cvrs_i$ is the CV of class i derived from remote sensing techniques; ET_i is the ET of class i (cm/day); $RSCV_w$ is the overall remote sensing based CV derived from the

weighted calculation procedure; w_i is the percentage of class i ; PET_t is potential evapotranspiration (cm) of date t .

Comparing these two methods of calculating the CV, the second method was the more traditional approach to specify the CV of each land use area, based on using reference values published in the GWLF manual, (Tung and Haith, 1995; Davis and Sorensen, 1969) then, similar to $RSCV$, calculate the overall CV (called $REFCV$). The equation for calculating $REFCV$ was as below:

$$REFCV = \sum_{i=1}^m cvref_i \times w_i \quad (25)$$

where, $REFCV$ is the overall CV determined by published reference; $cvref_i$ is the CV of class i derived from GWLF manual; w_i is the percentage of class i .

5.3.2. Weather generation

The Thiessen method was employed for the spatial integration of the seven point meteorological observations within the study area. This is a graphical method, adjusting for the non-uniform location of gauged stations by determining their area of influence. The method is based on the construction of areas of influence centered on each point measurement, the so-called Thiessen polygons. The measurement for each point is then

taken to be representative of the variable on its respective area of influence. The adjusting equations were as follows.

$$\begin{aligned} TEMP_{mean} &= \sum_{i=1}^n TEMP_i \times A_i \\ RAIN_{mean} &= \sum_{i=1}^n RAIN_i \times A_i \end{aligned} \quad (26)$$

where, $TEMP_{mean}$ is the integrated areal temperature ($^{\circ}C$); $TEMP_i$ is daily temperature of gauged station i ; $RAIN_{mean}$ is the integrated precipitation (cm); $RAIN_i$ is daily precipitation of gauged station i ; and A_i is influence coefficient of gauged station i .

A stochastic weather generation model (Tung and Haith 1995) was used to reflect possible variations in daily temperature and precipitation heights based on the local climate statistics from 1995~2002. Daily temperature was calculated using the first-order autoregressive equation given in Pickering et al. (1988) as follows.

$$TEMP_i = \mu_{Tm} + \rho(TEMP_{i-1} - \mu_{Tm}) + v_i \sigma_T \sqrt{1 - \rho^2} \quad (27)$$

where, $TEMP_i$ is the temperature on day i ; μ_{Tm} is the mean temperature for a period ($^{\circ}C$) (one month herein); ρ is the lag-one autocorrelation coefficient of temperature during

the period; ν is the normal sampling deviate between 0~1; σ_T is the standard deviation of temperature during the period.

Daily precipitation was determined by a conditional probability for the occurrence of wet and dry days based on the recorded climate sequences. Rainfall amount was generated as a logarithmic distribution function stated as below (Hong 1997):

$$RAIN_i = \mu_p(I) \times [-\ln(1 - RN)] \quad (28)$$

where, $RAIN_i$ is rainfall amount on day i (cm); $\mu_p(I)$ is the mean rainfall on month I (cm); and RN is a random number, the range of RN was “ $0 < RN < 1$ ”.

As for the simulation of future weather data, the normalized predictor variables which were exported from the CGCM1 model (The First Version of the Canadian Global Coupled Model; Flato et al. 2000) under SRES A2 and B2 experiments were selected to predict the possible climate change conditions. Scenario parameters acquired from the grid point N24.1°E120.0° on CGCM1 model was adopted in this study because the distance between the point and study area is the nearest.

The study procedures were as follows. First, we used the weather generation model

to generate a 100 year weather record based on the historic statistic. And then, two monthly means of CGCM1 outputs, such as the difference of temperature (ΔT) and the ratio of precipitation (RP), were applied to modify the generated weather sequence. Finally, the simulated future weather data was used to assess the impacts of short-term, mid-term and long-term climate change on watershed hydrology. The modified functions of weather data were stated as equations (29).

$$\begin{aligned} T'_{t,m} &= T_{t,m} + \Delta T_m \\ P'_{t,m} &= P_{t,m} \times RP_m \end{aligned} \tag{29}$$

where, $T'_{t,m}$ and $P'_{t,m}$ are the modified temperature and precipitation on day t ; $T_{t,m}$ and $P_{t,m}$ are the historic recorded temperature and precipitation on day t ; ΔT_m and RP_m are the difference of temperature and ratio of precipitation obtained from CGCM1 forecasts.

Table 1. Scenario parameters of the SRES-A2 experiment exported from the CGCM1 model (Tien, 2003)

Month	Difference in temperature (ΔT)			Ratio of precipitation (RP)		
	Short	Middle	Long	Short	Middle	Long
Jan	0.94	1.62	2.76	1.22	1.12	1.02
Feb	1.81	2.57	3.27	1.35	1.01	0.89
Mar	1.25	2.64	3.78	1.30	1.03	0.88
Apr	0.6	1.82	4.64	1.13	0.80	0.76
May	-0.46	2.78	4.54	1.10	0.82	0.54
June	1.09	3.62	5.62	1.03	0.79	0.70
July	1.18	2.26	4.52	0.92	0.93	0.70
Aug	0.52	2.05	3.45	1.19	1.03	1.23
Sept	0.45	1.9	3.12	1.18	0.97	1.29
Oct	0.43	1.81	2.68	0.92	0.99	1.09
Nov	0.47	2.1	2.53	1.10	1.24	0.80
Dec	1.41	2.43	2.81	0.96	0.88	0.69

Table 2. Scenario parameters of the SRES-B2 experiment exported from the CGCM1 model (Tien, 2003)

Month	Difference in temperature (ΔT)			Ratio of precipitation (RP)		
	Short	Middle	Long	Short	Middle	Long
Jan	1.14	1	0.83	1.36	1.71	1.65
Feb	1.45	0.91	1.01	1.48	1.81	2.54
Mar	1.18	0.97	0.95	0.71	2.44	3.26
Apr	1.15	0.98	0.85	0.62	2.28	3.09
May	0.83	0.95	0.77	1.69	1.76	2.75
June	0.76	1.18	0.95	2.6	1.72	3.18
July	0.96	0.97	0.97	1.59	1.47	2.6
Aug	1.12	1.07	1.26	0.72	1.16	1.84
Sept	1.07	1.04	1.19	0.73	1.28	1.8
Oct	1.02	1.08	1.39	1.11	1.37	1.58
Nov	0.82	0.94	1	0.55	1.72	1.8
Dec	0.94	0.56	0.76	1.6	1.3	2.63

5.3.3. Assessment of the effects of CV on stream flow simulations

Stream flow simulations were performed using the two types of calculated CV values, to investigate the effect of CV parameters on the GWLF simulations. The processes were as follows:

First, the daily temperature and precipitation exported from the weather generation model based on the historic climate statistics, and CV's calculated from different methods as above were substituted into the GWLF model to simulate the stream flows based on current conditions. Then, the observed stream flow records taken from the Shang-Guei-Shan-Ciao gauged station were applied to investigate the simulated accuracy of the simulation using regression analysis.

5.3.4. Predictions of land-use change and future CV values

The land-use status in 2030 of short-term, 2058 of mid-term, and 2086 of long-term future were predicted to represent the land-use conversions in the next three periods (28 years each). Furthermore, the results were integrated with the climate change data exported from the CGCM1 model to simulate the future values of CV according to equation (23) and (24). The predicted time stages for future land-use conversions and CV values were shown in Figure 10.

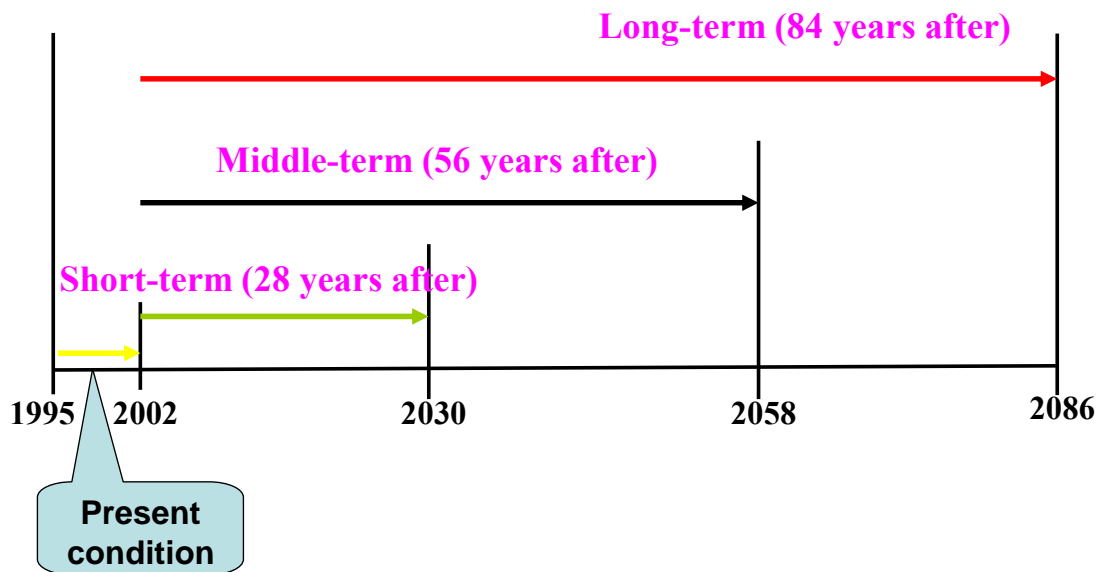


Figure 10. The predicted time stages for future land-use conversions and CV values

Two assumptions were made in the calculation of future land-use status and CV values. The first assumption was that the land-use change of north Taiwan was constant. Under this assumption, the Markov model was applied to predict the percent of each land-use type using a transition probability matrix considering the land-use change from 1995 to 2002. The second assumption was that the ET of land-use types was invariable in the future. This simplification allowed us to estimate a CV which was determined by the land-use status as shown in equation (23) and (24). Finally, the actual ET estimated from remote sensing, the PET calculated using the future temperature, and the land-use change projected by the Markov model were integrated together to calculate the future CV value. Simulations of future CV values were shown as equations (25) and (26).

$$fcvrs_i = \frac{ET_i}{FPET_i} \quad (25)$$

$$FRSCV_w = \sum_{i=1}^m fcvrs_i \times w_i \quad (26)$$

where, $fcvrs_i$ is the future CV of class i derived from remote sensing techniques; ET_i is the ET of class i (cm/day); $FRSCV_w$ is the future values of overall remote sensing based CV derived from the weighted calculation procedure; w_i is the percentage of class i ; $FPET_i$ is future potential evapotranspiration (cm/day).

5.3.5. Effects of land-use status and ET parameters on future stream flow simulation

Future temperature and precipitation defined by the SRES scenario were entered into the GWLF model to predict the stream flows based on climate change condition using various land-use and CV parameters. The objective of this process was to compare the difference of simulated flows between two approaches. The first approach is the traditional approach. Current land-use data was adopted and the CV parameters were acquired from the published references without considering its future change. Both parameters were assumed to be consistent during the simulated procedures. In the proposed approach, future land-use data was projected using the Markov model and the future CV values were derived from the integration of SEBAL model, CGCM1 model, and Markov model. A parameter comparison between two methods is shown in Table 3.

Table 3. A parameter comparison between traditional approach and proposed approach used in this study

Methods	Climate change simulation	Land-use status	ET parameter (CV value)
Traditional approach	CGCM1 model, SRES scenario	Without considering land-use change, only adopted the current land-use data directly.	CV values were acquired from the published references and without considering their future change.
Proposed approach	CGCM1 model, SRES scenario	Future land-use status was predicted using the Markov model.	Future CV values were derived from the integration of SEBAL model, CGCM1 model, and Markov model.

5.4. Assessment of Future Impacts on Hydrological Cycle of North Taiwan

Flow series from 1995 to 2002 was generated from the GWLF model and taken as the baseline of the current hydrological condition. The simulated stream flows between future and current conditions were compared for assessing the impacts of short-term, mid-term and long-term climate change, land-use change and ET change on the hydrology of north Taiwan.

6. RESULTS

6.1 Comparison of ET Difference among Various Land-use Types

6.1.1. Land-use classification of north Taiwan

The study area was classified into seven categories using the hybrid classification method, forest, building, farmland, fallow farmland, water, cloud, and shadow. To assess the classification accuracy, national land-use inventory data from 1995 was first combined to fit the objective categories and applied to compare with the generated maps. Excluding shadow and cloud, two test areas for each land-use type were selected and used to calculate the classified accuracy based on these examinations. Spatial distribution of the selected blocks and test areas is shown as Figure 11; classification of the test area is shown as Table 4; accuracy assessment of the land-use classification of November 25, 1995 is calculated in Table 5.

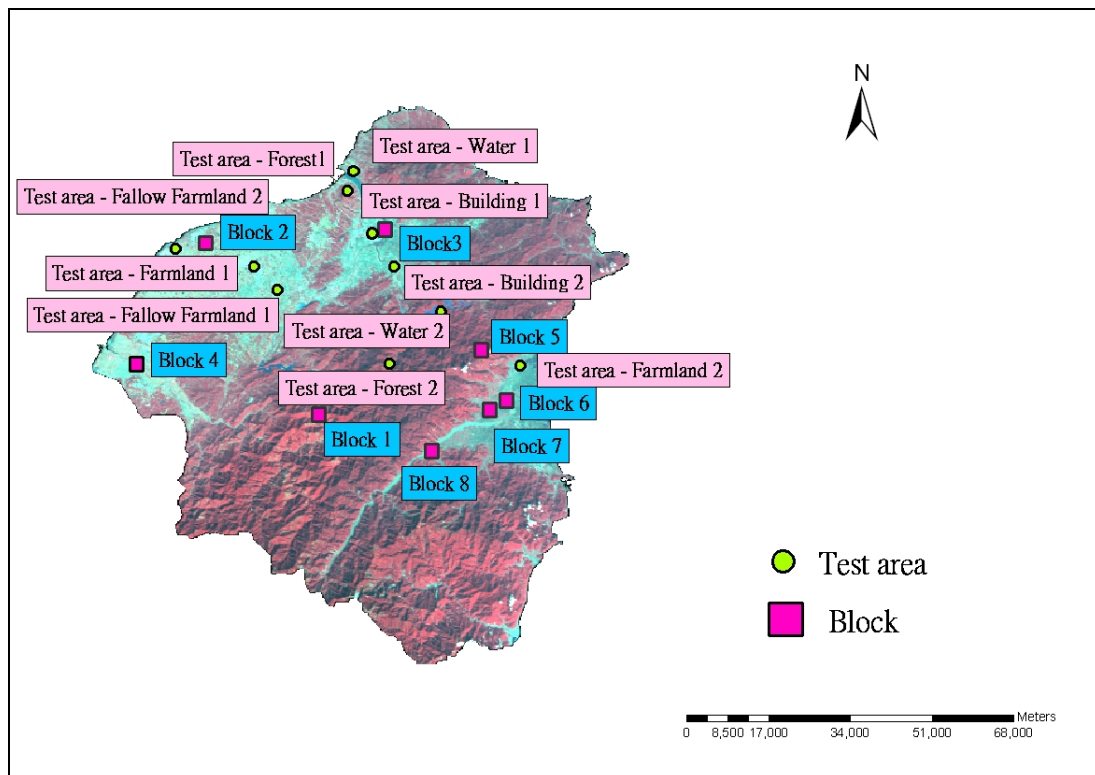


Figure 11. Spatial distribution of the selected blocks and test areas

(The size of each block is 100 ha, which was extracted from each landsat image. As for the test area, the size for forest1, forest2, building1, building2, water1, water2, farmland1, and farmland2 is 140.40ha, 694.71ha, 563.04ha, 376.83ha, 161.46ha, 439.02ha, 206.88ha, and 1020.78ha, respectively.)

Table 4. Classification of test areas







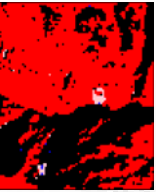
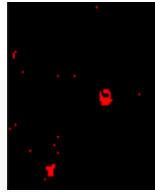


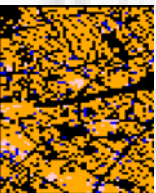
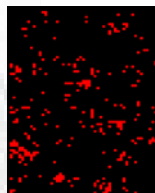

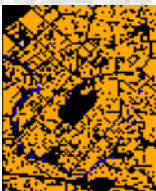
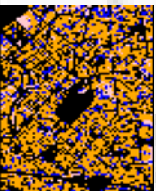
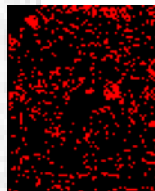

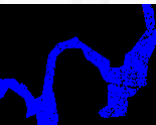
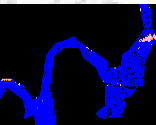
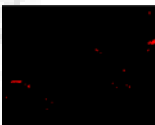



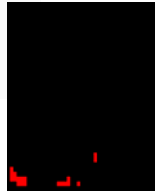




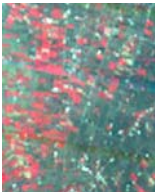


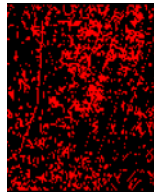
Land-use type	Satellite image	Ground truth	Image classification	Image subtraction
Forest 1				
Forest 2				
Building1				
Building2				
Water 1				
Water 2				
Farmland1				
Farmland2				

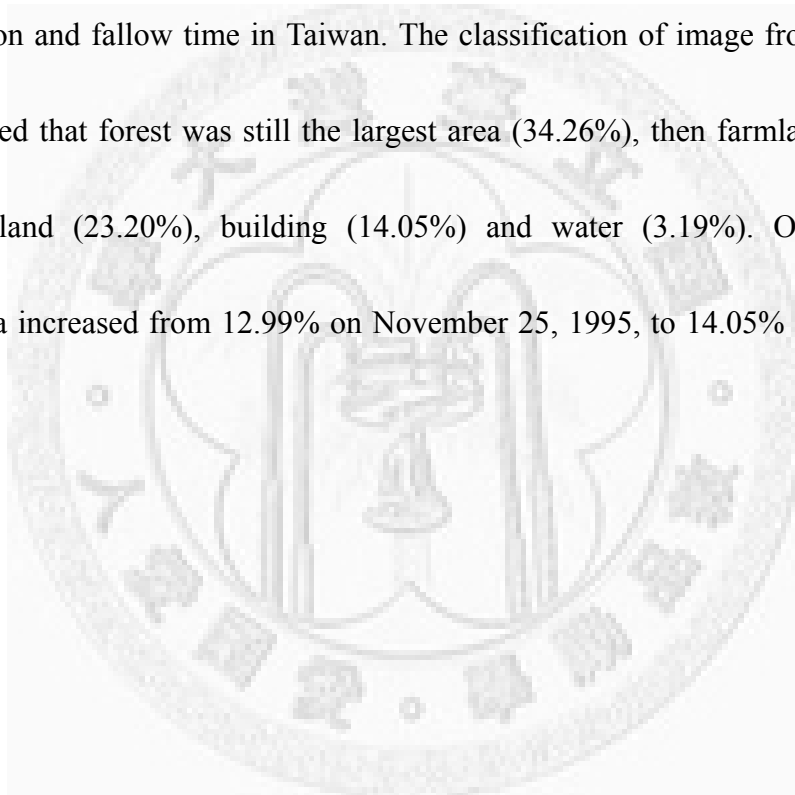
Table 5. Examination of the land-use classification of November 25, 1995

Land type	Forest	Building	Water	Farmland	Fallow Farmland	Total	User's accuracy
Forest	9144	0	0	128	7	9279	98.55%
Building	0	9212	414	221	596	10443	88.21%
Water	0	27	6539	3	103	6672	98.01%
Farmland	281	1031	97	6558	75	7762	84.49%
Fallow Farmland	11	1466	186	0	4212	5875	71.69%
Total	9306	11711	7186	7190	4918	40031	
Producer's accuracy	98.26%	78.66%	91.00%	91.21%	85.64%		
Overall accuracy = 89.09%							
Kappa statistic = 0.8525							

Table 4 and Table 5 show that most errors occurred when categorizing fallow farmland. This might be due to the fact that building and fallow farmland both have similar characteristics on spectral reflectance making the two types difficult to separate well. However, the accuracy of forest, buildings, water, and farmland was 98.55%, 88.21%, 98.01%, and 84.49%, respectively. The overall accuracy was about 89.09%, suggesting that hybrid classification is a suitable approach to generate a land-use map. The same procedures were adopted to create the land-use maps of north Taiwan on July 20, 1995 and January 4, 2002, and the results are shown in Figure 12. Further to gather the statistics of pixel numbers and percentages of five land-use types, the result is shown in Table 6.

A further comparison of land-use status among three different dates indicated that

in July 1995, forest occupied most of the study site (37.78%), then farmland (36.71%), building (10.58%), fallow farmland (7.52%), and water (7.41%) was smaller. In November 1995, forest has the largest area (35.89%), then farmland (22.39%), fallow farmland (21.88%), building (12.99%), and water (6.85%). The results showed that there was a significant transition between the farmland and fallow farmland because of the cultivation and fallow time in Taiwan. The classification of image from January 4, 2002, revealed that forest was still the largest area (34.26%), then farmland (25.25%), fallow farmland (23.20%), building (14.05%) and water (3.19%). Obviously, the building area increased from 12.99% on November 25, 1995, to 14.05% on January 4, 2002.



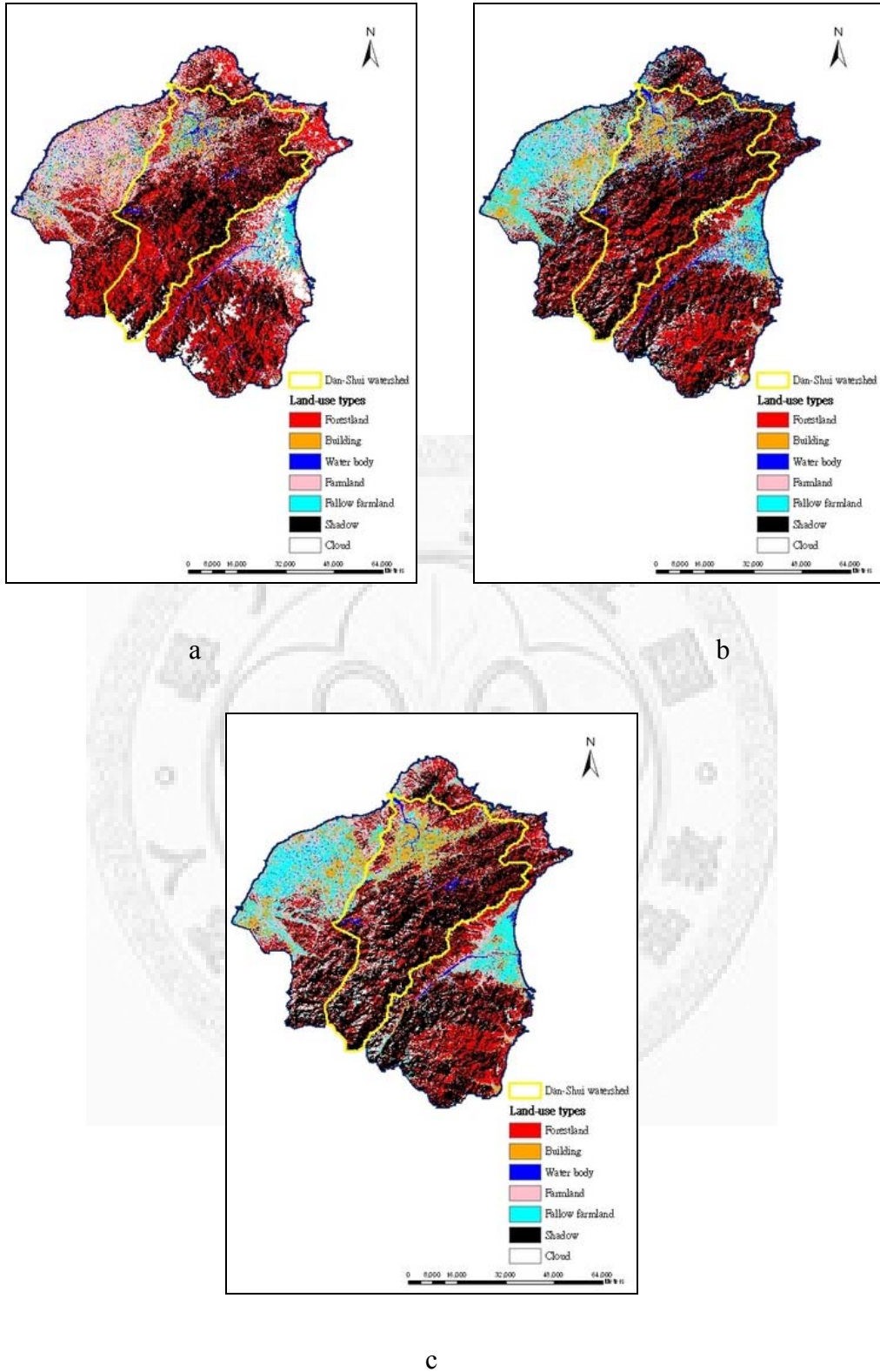


Figure 12. Land-use maps generated by the hybrid classification

(a: July 20, 1995; b: November 25, 1995; c: January 4, 2002)

Table 6. Pixel number and percentages of five land-use types

Land-use types	July 20, 1995		November 25, 1995		January 4, 2002	
	Pixel number	Percentage	Pixel number	Percentage	Pixel number	Percentage
Forest	2075851	37.78%	1971918	35.89%	1882195	34.26%
Building	581463	10.58%	713486	12.99%	772093	14.05%
Wate	407305	7.41%	376406	6.85%	175180	3.19%
Farmland	2016862	36.71%	1230342	22.39%	1387287	25.25%
Fallow farmland	412923	7.52%	1202252	21.88%	1277649	23.25%
Total	5494404	100%	5494404	100%	5494404	100%

6.1.2. Estimation of the daily actual ET using remote sensing

Figure 13 and Figure 14 present the generated maps of energy balance parameters and actual ET of July 20 and November 25, 1995 using SEBAL model (only five major parameters such as NDVI, surface temperature, soil heat flux, sensible heat flux and actual ET are shown here). When forestland is compared to other types of land-use, it had the higher value of NDVI and actual ET, and had the lower value of surface temperature, soil heat flux and sensible heat flux. A comparison of parameters between the two time periods, confirmed that surface temperature, NDVI and actual ET had higher values in July, and sensible heat flux and soil heat flux had higher values in November. Knapp (1985) stated that “Seasonal trends of evapotranspiration within a given climatic region follow the seasonal declination of solar radiation and the resulting air temperatures. Minimum evapotranspiration values generally occur during the coldest months of the year. Maximum values generally coincide with the summer season.” In our study, ET in summer revealed the highest value (July 20, 1995: 0.531 cm/day) and the lowest value in winter (January 9, 1995; 0.233 cm/day). The result showed the similar trend with previous study.

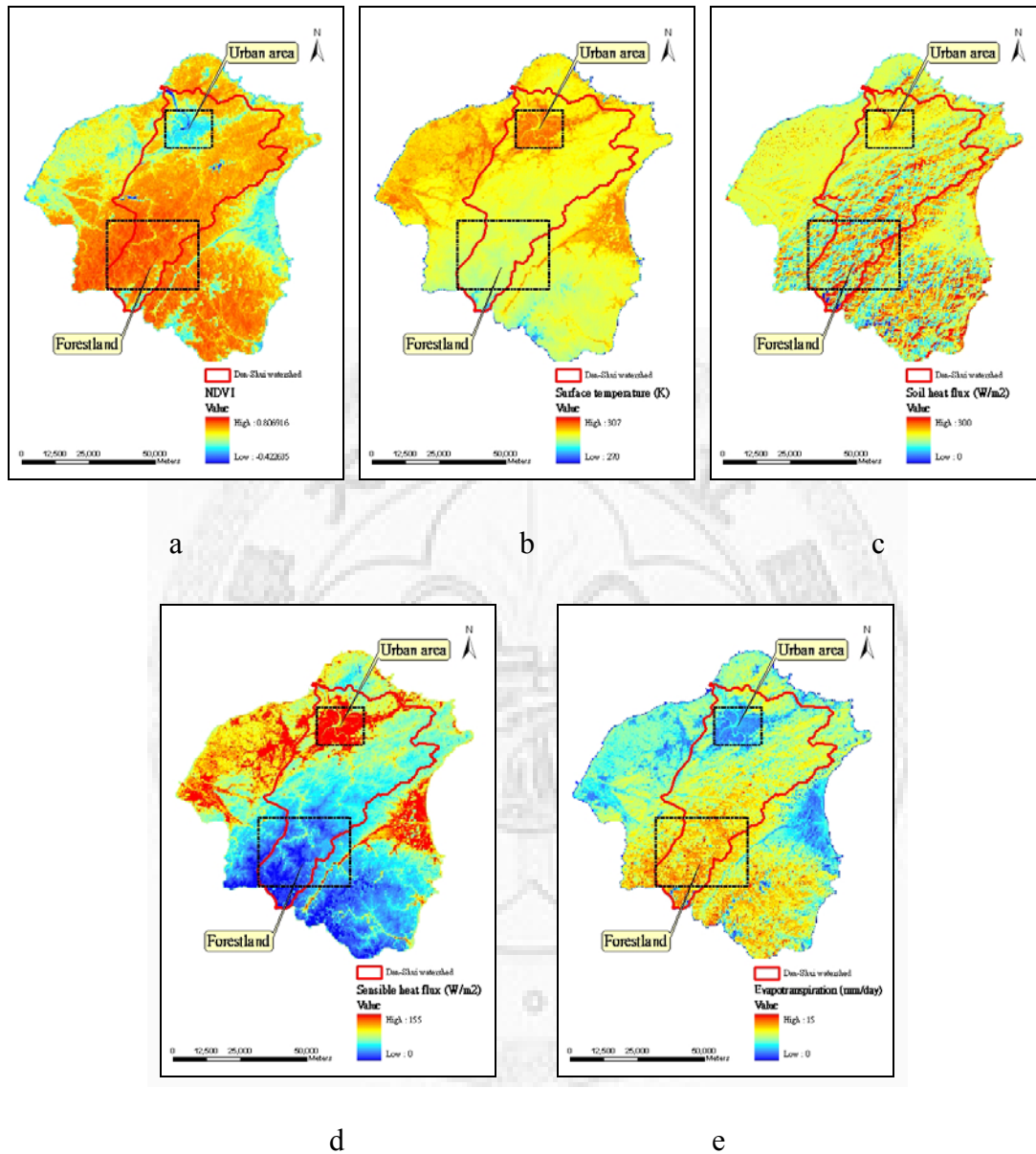


Figure 13. Estimated energy balance parameters and ET maps of July 20, 1995

(a: NDVI; b: surface temperature; c: soil heat flux; d: sensible heat flux; e: ET)

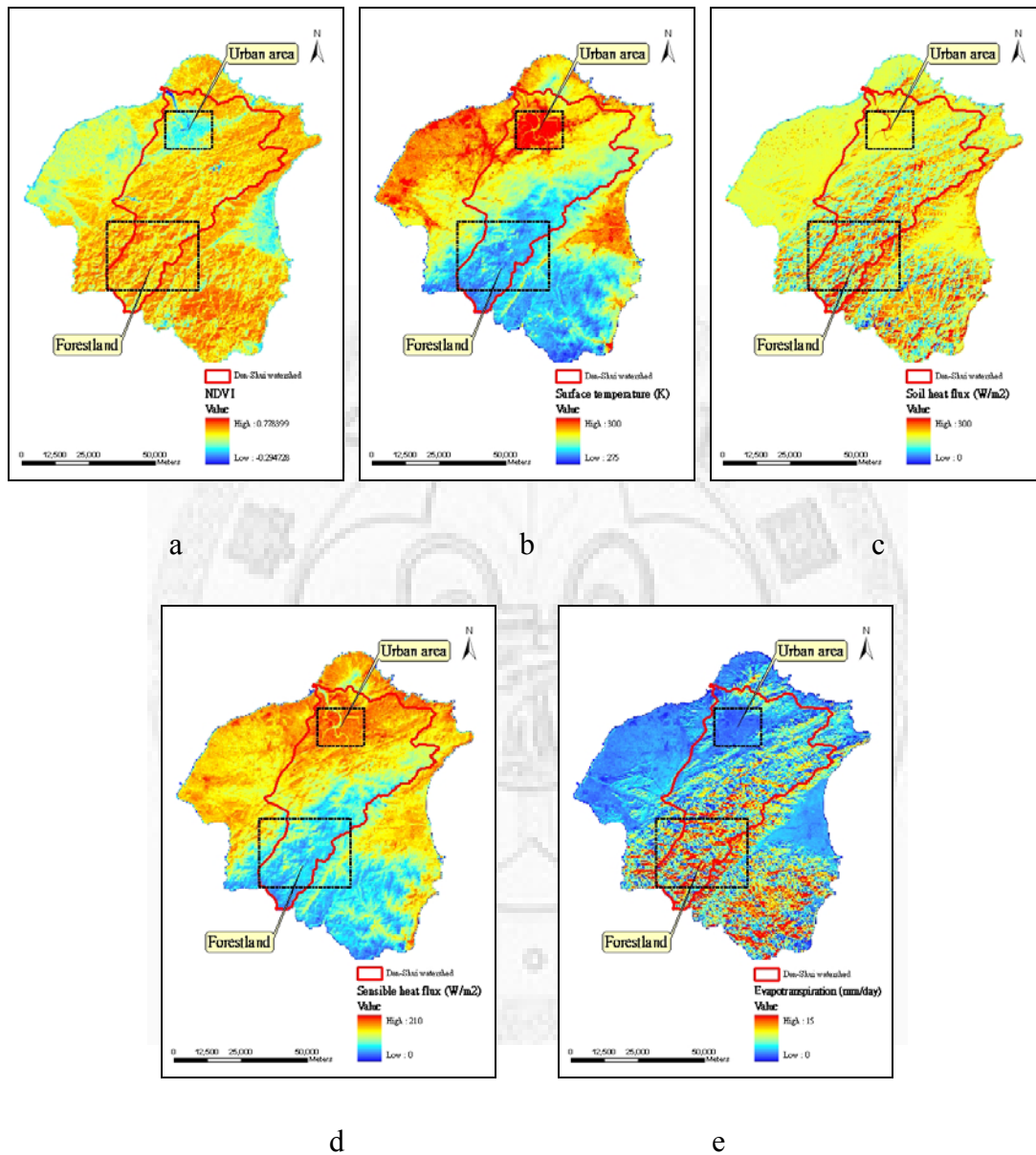


Figure 14. Estimated energy balance parameters and ET maps of November 25, 1995

(a: NDVI; b: surface temperature; c: soil heat flux; d: sensible heat flux; e: ET)

6.1.3. Difference of ET among various land-use types

ET among five land-use types is computed in Table 7. In July, forest had the highest mean daily ET value (0.723cm/day), then farmland (0.530cm/day), water (0.281cm/day), fallow farmland (0.267cm/day), and building (0.220cm/day); During November, consistently forest was consistently the highest value (0.395cm/day), then farmland (0.185cm/day), fallow farmland (0.139cm/day), water (0.113cm/day), and building (0.088cm/day).

Table 7. Computation of ET (cm/day) of five land-use types in 1995

	Forest	Building	Water	Farmland	Fallow farmland
July 20	0.723 ± 0.227	0.220 ± 0.048	0.281 ± 0.045	0.530 ± 0.159	0.267 ± 0.042
November 25	0.395 ± 0.148	0.088 ± 0.024	0.113 ± 0.020	0.185 ± 0.054	0.139 ± 0.043

6.2. Effect of Ecosystem Classification Systems at Various Spatial Scales on Environmental Parameters

Table 8 presents the results after the stepwise discriminant analysis. They indicated that the required parameters and the numbers of parameters for discriminating five land-use types varied with different ecosystem classification systems at various scales. Considering unit 3 and unit 2 of the watershed division as an example, it is clear that

both units have different required parameters and numbers of parameters when discriminating five land-use types. For example, unit 3 and unit 2 are located in a flat plain and a steep mountainous area, respectively. The results indicate that unit 2 has four parameters ($NDVI$, z_{om} , ε_0 , α_0) and unit 3 has eleven parameters (r_{ah} , ε_0 , $NDVI$, H , T_0 , z_{om} , τ_{sw} , ET_{24} , p_{air} , R_n , $\cos\theta$). The reasons for the different numbers may result from the characteristics of the ecosystem units. As stated previously, ecosystem units have unique characteristics for climate, terrain or ecological conditions. This characteristic may influence the calculation of environmental parameters and indirectly affect the result of stepwise discriminant analysis.

No matter what kind of spatial scales and ecosystem classification systems were used, both $NDVI$ and ε_0 parameters were extracted in the stepwise discriminant analysis, which suggests that these two parameters can be regarded as the most significant factors.

Table 8. Stepwise discriminant analysis under different ecosystem classification systems at various scales

Spatial scales		Selected parameters
North Taiwan		$NDVI$ z_{om} ε_0 α_0 R_n G_o r_{ah} p_{air} τ_{sw} u^*
Geographic climate method	Unit 1	$NDVI$ T_0 ε_0 α_{toa} z_{om} r_{ah} H u^* τ_{sw} α_0 ET_{24} R_n Ra_{24} G_o
	Unit 2	$NDVI$ T_0 z_{om} r_{ah} ε_0 u^* α_0 G_o R_n H τ_{sw} α_{toa} ET_{24}
	Unit 3	$NDVI$ z_{om} ε_0 r_{ah} α_0 $cos\theta$ H G_o R_n ET_{24}
	Unit 4	$NDVI$ T_0 z_{om} r_{ah} ε_0 G_o α_0 R_n u^* H τ_{sw}
	Unit 5	z_{om} T_0 u^* $cos\theta$ H $NDVI$ τ_{sw} α_0 G_o R_n r_{ah} ε_0
	Unit 6	$NDVI$ z_{om} T_0 u^* r_{ah} ε_0 R_n ET_{24} α_0 α_{toa} G_o
	Unit 7	z_{om} $cos\theta$ $NDVI$ T_0 H τ_{sw} ε_0 u^* r_{ah}
	Unit 8	z_{om} T_0 H G_o α_{toa} ε_0 $NDVI$ τ_{sw} u^* r_{ah} R_n
	Unit 9	$NDVI$ ε_0 T_0 $cos\theta$ τ_{sw} α_0 H z_{om}
	Unit 10	$NDVI$ T_0 τ_{sw} ε_0 z_{om} r_{ah} u^* G_o α_0 R_n
	Unit 11	$NDVI$ T_0 ε_0 H α_0 τ_{sw} z_{om} u^* τ_{sw} r_{ah} G_o R_n
	Unit 12	$NDVI$ T_0 τ_{sw} $cos\theta$ ε_0 G_o R_n α_0 α_{toa} Ra_{24} p_{air} H z_{om}
Watershed division method	Unit 1	$NDVI$ ε_0 z_{om} r_{ah} G_o $cos\theta$ p_{air} R_n Ra_{24}
	Unit 2	$NDVI$ z_{om} ε_0 α_0
	Unit 3	r_{ah} ε_0 $NDVI$ H T_0 z_{om} τ_{sw} ET_{24} p_{air} R_n $cos\theta$
	Unit 4	z_{om} $NDVI$ ε_0 T_0 Ra_{24} α_0 R_n u^* r_{ah} H τ_{sw} G_o ET_{24}
	Unit 5	$NDVI$ z_{om} ε_0 u^* r_{ah} T_0 ET_{24}
	Unit 6	$NDVI$ r_{ah} τ_{sw} u^* ε_0 G_o R_n H p_{air} Ra_{24}
	Unit 7	$NDVI$ ε_0 z_{om} α_0 r_{ah} G_o $cos\theta$ α_{toa}

6.3. Assessment of Future Land-Use Status and ET Change on Stream Flow Simulation under Climate Change Conditions

6.3.1. Calculations of CV under present condition

Figure 15 illustrates the Thiessen polygon divisions and the influence coefficients for the seven meteorological stations. These coefficients were adopted to integrate the historical temperature and precipitation observations collected from seven gauged stations for deriving a weather series which involved the climatic characteristics of the whole of north Taiwan. The mean daily temperature, saturated water vapor pressure and potential evapotranspiration on July 20 and November 25, 1995, were then calculated from the integrated weather data and shown as Table 9.

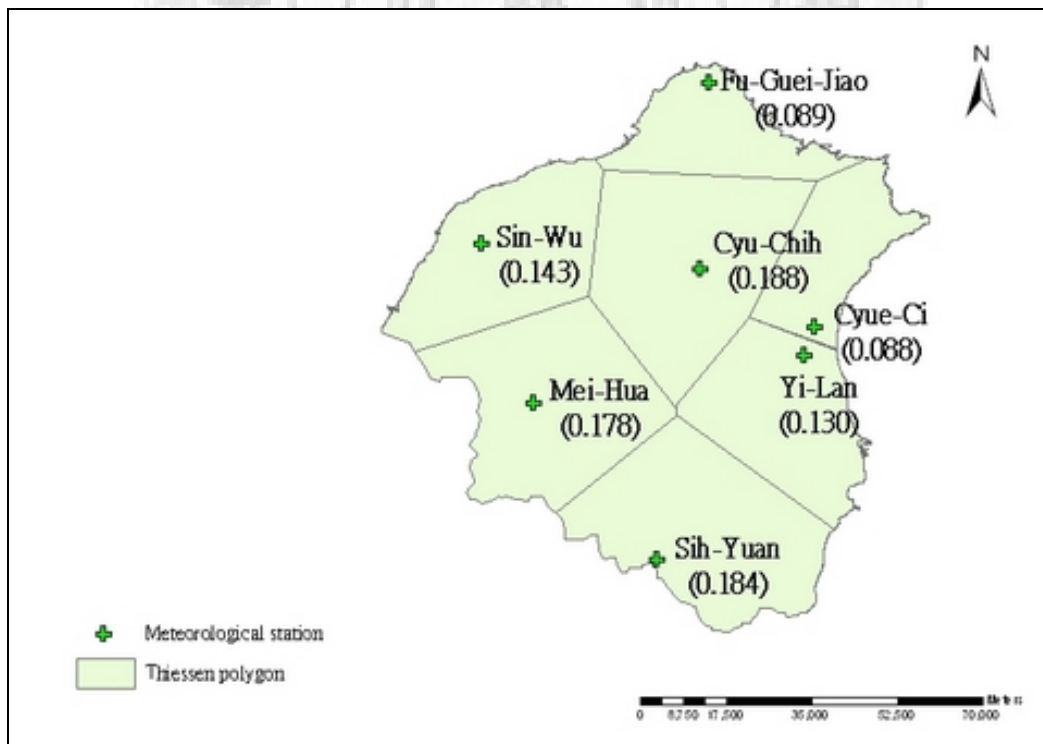


Figure 15. Thiessen polygons and their influence coefficients

Table 9. Mean daily temperature, saturated water vapor pressure and potential evapotranspiration on July 20 and November 25, 1995

	Mean daily temperature (°C)	e_{0t} (mb)	PET (cm)
July 20 (wet season)	26.268	33.905	0.427
November 25 (dry season)	14.390	31.523	0.274

Table 10 and Table 11 are the CV values obtained from the proposed remote sensing using various procedures; Table 12 is the CV calculated from the traditional approach. From Table 10 and Table 11, the remote sensing-based CV derived from various procedures showed similar results ($RSCV_d$: 1.243 and 0.850; $RSCV_w$: 1.245 and 0.851). Due to the advantage of $RSCV_w$ on future CV calculation, it was applied in further hydrologic simulations instead of $RSCV_d$.

Comparing Table 11 with Table 12, the calculated CVs of the wet season ($RSCV_w$: 1.245; $REFCV$: 0.842) were higher than the value of the dry season ($RSCV_w$: 0.851; $REFCV$: 0.717). Regardless of whether it was the wet season or the dry season, the CV values derived from the remote sensing approach (wet season: 1.245; dry season: 0.851) were larger than those from the traditional approach (wet season: 0.842; dry season: 0.717). To reconfirm this situation and to validate the following stream flow model, the Dan-Shui watershed was selected for more detail analysis. The results of the calculated

CVs for Dan-Shui were similar; that is, the remote sensing approach (wet season: 1.518; dry season: 0.983) remained a larger CV value than the traditional approach (wet season: 0.826; dry season: 0.754).

Table 10. CV obtained from the remote sensing using the direct calculation procedure

$RSCV_d (=ET/PET)$	
$RSCV_d$ of July 20 (for wet season)	$0.531 / 0.427 = 1.243$
$RSCV_d$ of November 25 (for dry season)	$0.233 / 0.274 = 0.850$

Table 11. CV obtained from the remote sensing using the weighted procedure

	Forest	Building	Water	Farmland	Fallow farmland
$cvrs$ of July 20	1.69	0.51	0.66	1.24	0.63
$RSCV_w$ of July 20 (for wet season)	$1.69 \times 0.3778 + 0.51 \times 0.1058 + 0.66 \times 0.0741 + 1.24 \times 0.3671 + 0.63 \times 0.0752 = 1.245$				
$cvrs$ of November 25	1.44	0.32	0.41	0.67	0.51
$RSCV_w$ of November 25 (for dry season)	$1.44 \times 0.3589 + 0.32 \times 0.1299 + 0.41 \times 0.0685 + 0.67 \times 0.2239 + 0.51 \times 0.2188 = 0.851$				

Table 12. CV obtained from the traditional approach

	Forest	Building	Water	Farmland	Fallow farmland
$cvref$	1	0	1	1	0.3
$REFCV$ of July 20 (for wet season)	$1 \times 0.3778 + 0 \times 0.1058 + 1 \times 0.0741 + 1 \times 0.3671 + 0.3 \times 0.0752 = 0.842$				
$REFCV$ of November 25 (for dry season)	$1 \times 0.3589 + 0 \times 0.1299 + 1 \times 0.0685 + 1 \times 0.2239 + 0.3 \times 0.2188 = 0.717$				

6.3.2. Validation of stream flow simulation

The Dan-Shui watershed was also used to validate the GWLF model. The CV values obtained from two approaches were applied to assess their effects on stream flow simulations using the GWLF model. To validate the weather generation model, the following Table compared the historical records and simulated values. The Table showed that the correlation coefficient was higher than 0.99. Intercept and slope were approaching to “zero” and “one”, respectively. Therefore, the simulated weather records can be adopted for the GWLF simulation.

Table 13. Comparison between the observed and simulated temperature data

station	Cyu-Chih	
	observed	simulated
January	15.63	15.7
February	15.7	16.02
March	18.59	18.24
April	21.54	21.24
May	24.1	24.32
June	26.83	27.28
July	28.17	27.79
August	28.1	28.02
September	25.91	26.16
October	23.89	24.42
November	20.31	20.18
December	17.25	18.02
Correlation coefficient	0.99684	
Intercept	-0.25652	
Slope	1.006389	

The basis of setting model parameters was as follows. First, the values of CN₂ for five land-use types were derived from the user’s manual of the GWLF model, as

follows, 63 for forest, 98 for building, 98 for water, 79 for farmland and 70 for fallow farmland. The recession coefficient was adopted from the advice of Li et al., (2006) using a set value of 0.1. Daylight hours, which were related to the latitude of study area, were also given in the GWLF user's manual as shown in Table 14. Figure 16 is the generated map of seven land-use types of the Dan-Shui watershed in July, 20 and November, 25, 1995. From the classification map, clear shadow and cloud excluded from further analysis, and Table 15 shows the area and percentages of the five remaining land-use types in two periods. The result revealed that forestland occupied most of the Dan-Shui watershed (July 20: 51.53 %, November 25: 48.83 %). Finally, Figure 17 presents the estimated ET maps. RSCV and REFCV of the Dan-Shui watershed in wet and dry seasons are calculated in Table 16 and Table 17. The CV values obtained from remote sensing (wet season: 1.518; dry season: 0.983) and the reference manual (wet season: 0.826; dry season: 0.754) were applied in the following hydrologic simulations.

Table 14. Mean number of daylight hours in the study area (hours)

Month	Mean number of daylight hours
January	10.7
February	11.2
March	11.9
April	12.6
May	13.1
June	13.4
July	13.3
August	12.8
September	12.1
October	11.4
November	10.9
December	10.6

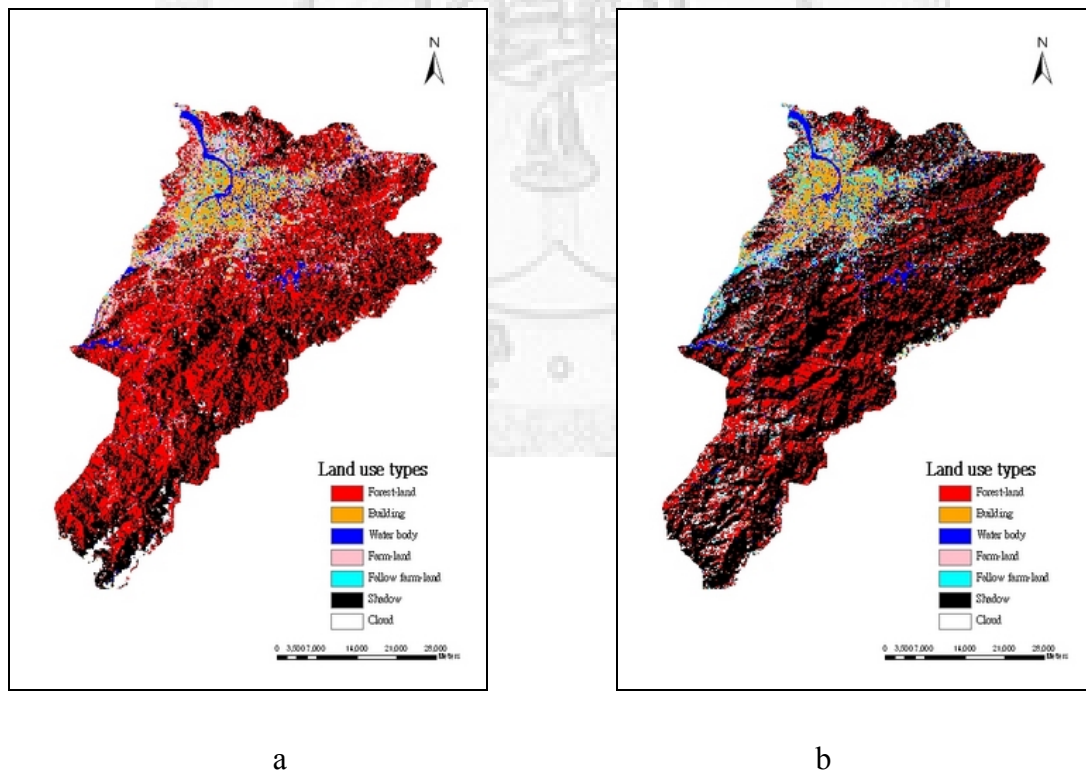


Figure 16. Land-use maps of the Dan-Shuei watershed from 1995

(a: July 20; b: November 25)

Table 15. Numbers of pixel and percentages of five land-use types of the Dan-Shui watershed (Excluding shadow and cloud types in both periods)

Land-use types	July 20, 1995		November 25, 1995	
	Pixel number	Percentage of each land-use	Pixel number	Percentage of each land-use
Forest	860157	51.53%	814997	48.83%
Building	237603	14.24%	260744	15.62%
Water	142952	8.56%	165368	9.90%
Farmland	353850	21.20%	213600	12.80%
Fallow farmland	74601	4.47%	214454	12.85%
Total	1669163	100%	1669163	100%

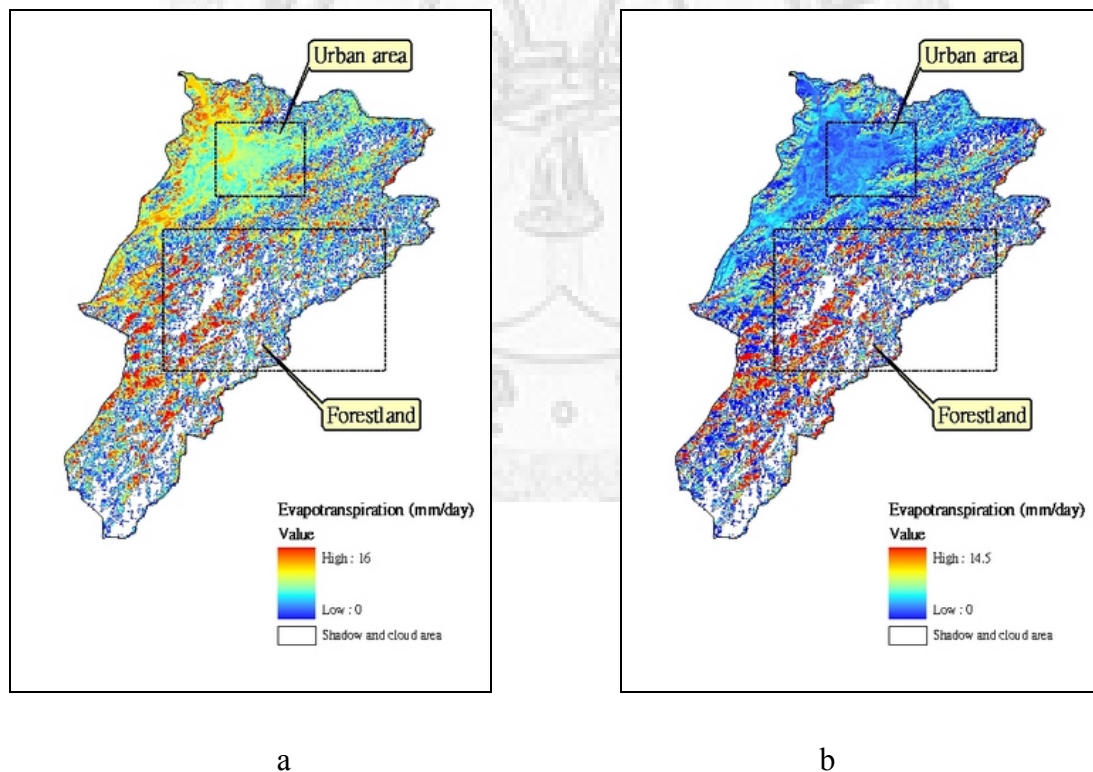


Figure 17. ET maps of the Dan-Shuei watershed from 1995

(a: July 20; b: November 25)

Table 16. *RSCV* calculations of the Dan-Shui watershed in wet and dry seasons

	Forestland	Building	Water body	Farmland	Fallow farmland
<i>cvrs</i> of July 20	1.98	0.62	0.87	1.39	0.91
<i>RSCV_w</i> of July 20 (for wet season)	$1.98 \times 0.5153 + 0.62 \times 0.1424 + 0.87 \times 0.0856 + 1.39 \times 0.2120 + 0.91 \times 0.0447 = 1.518$				
<i>cvrs</i> of November 25	1.58	0.22	0.26	0.60	0.58
<i>RSCV_w</i> of November 25 (for dry season)	$1.58 \times 0.4883 + 0.22 \times 0.1562 + 0.26 \times 0.0990 + 0.60 \times 0.1280 + 0.58 \times 0.1285 = 0.983$				

Table 17. *REFCV* calculations of the Dan-Shui watershed in wet and dry seasons

	Forestland	Building	Water body	Farmland	Fallow farmland
<i>cvref</i>	1.0	0	1.0	1.0	0.3
<i>REFCV</i> of July 20 (for wet season)	$1.0 \times 0.5153 + 0 \times 0.1424 + 1.0 \times 0.0856 + 1.0 \times 0.2120 + 0.3 \times 0.0447 = 0.826$				
<i>REFCV</i> of November 25 (for dry season)	$1.0 \times 0.4883 + 0 \times 0.1562 + 1.0 \times 0.0990 + 1.0 \times 0.1280 + 0.3 \times 0.1285 = 0.754$				

The daily temperature and precipitation exported from the weather generation model based on the climate statistics of the Cyu-Chih station from 1995 to 2002 were entered into the GWLF model with the above parameters to calculate the flow series. The results are shown as Table 18 and Figure 18. A regression analysis was used to investigate the relationship between the observed and calculated flow series. The results indicated that the regression coefficient was 0.877 when using *RSCV_w*, and 0.853 for the use of *REFCV*. Such a high regression coefficient implies that, even though the

simulated values are overestimates compared with the observed values, the CV value obtained from the proposed remote sensing approach could represent truer stream flow characteristics than the traditional approach. In other words, the use of the remote sensing approach to derive the parameters for the GWLF model was more suitable to simulate the hydrological flow in north Taiwan.

Table 18. Observed and simulated stream flow values (cm/month) of the Dan-Shui watershed

Month	Observed value	Simulated value (Using <i>REFCV</i>)	Simulated value (Using <i>RSCV</i>)
January	2.31	7.9	6.7
February	7.43	15.5	14.4
March	6.37	12.1	10.7
April	2.56	13.1	11.5
May	5.78	14.8	11.8
June	10.17	27.7	20.3
July	13.62	24.3	17
August	17.96	18.8	15.3
September	51.65	46.5	40
October	19.90	29.6	24.2
November	21.93	13.8	10.7
December	9.63	14.4	11.4
Total	169.30	238.50	194.00
Average	14.11	19.88	16.17

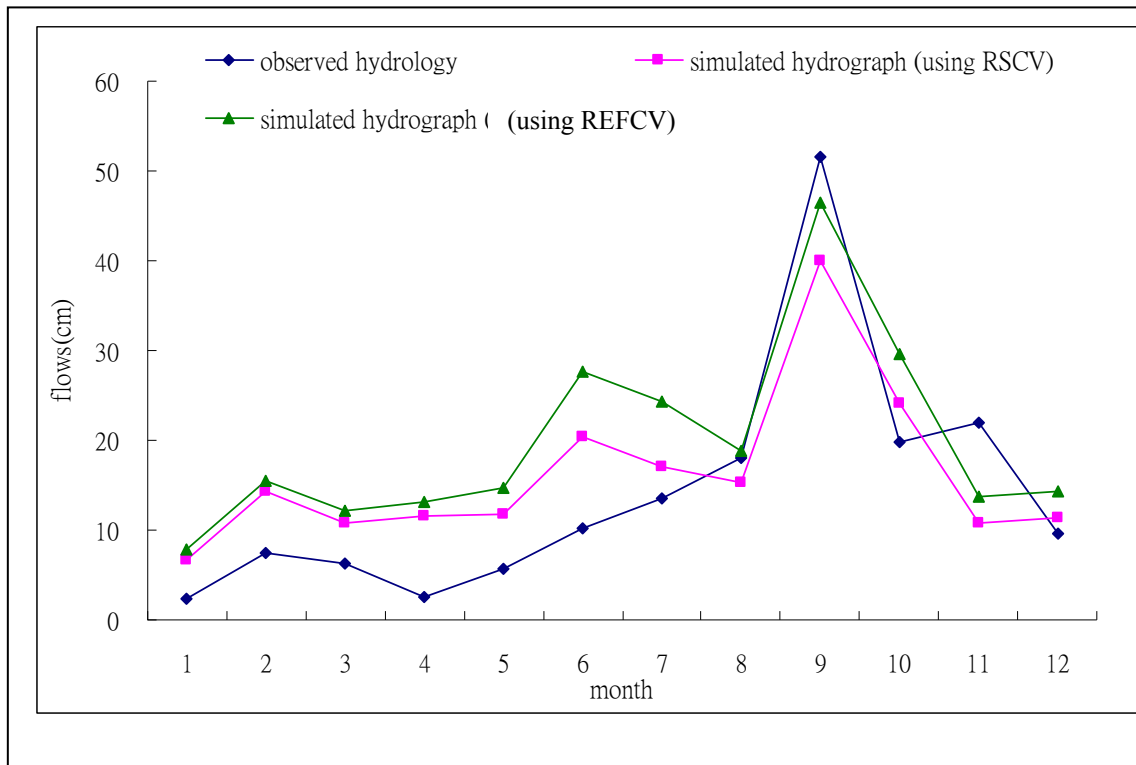


Figure 18. The observed and simulated hydrographs

6.3.3. Assessment of Future Land-Use Status and ET Change on Stream Flow Simulation under Climate Change Conditions

The transition matrix of the observed land-use changes based on the land-use maps on November 25, 1995 and January 4, 2002 is shown in Table 19. Goodman's Chi-squared statistic for the two periods ($\chi^2 = 76742.52$) was larger than the reference value ($\chi^2 = 32.00$) and was statistically very significant ($p \ll 0.001$), indicating that the processes of land-use transition during the periods are not random. Moreover, to

validate the Markov projection, the calculated transition probability matrix was used to predict the land use in 2002. It was then compared with the image classification of 2002 using regression analysis. The result was shown as Table 20. Clearly correlation coefficient was higher than 0.96 even though the predicted result was not exactly the same with the image classification. From above validation, integrating the Markov model and remote sensing technique for future land-use prediction should be feasible.

Table 19. Transitional pixels and probabilities from 1995 to 2002

Transition from row to column	Forest	Building	Water	Farmland	Fallow farmland	Column total (1995 distribution)
Forest	274 (0.823)	2 (0.006)	0	44 0.132	13 (0.039)	333
Building	0	86 (1)	0	0	0	86
Water	2 (0.033)	17 (0.283)	13 (0.217)	13 (0.217)	15 (0.250)	60
Farmland	34 (0.143)	18 (0.076)	1 (0.004)	121 (0.508)	64 (0.269)	238
Fallow farmland	14 (0.059)	33 (0.139)	7 (0.030)	80 (0.338)	103 (0.435)	237
Row total (2002 distribution)	324	156	21	258	195	954

The numbers in parentheses indicate the transitional probability.

Table 20. Validation of Markov prediction

	Land classification	Markov prediction	Difference
Forest	34.23%	32.80%	-1.43%
Building	16.11%	20.52%	4.41%
Water	3.16%	2.32%	-0.84%
Farmland	23.95%	25.09%	1.14%
Fallow farmland	22.55%	19.27%	-3.28%
Total	100.00%	100.00%	
Correlation coefficient		0.9668	
Intercept		0.0028	
Slope		0.9861	

For climate change simulation, IPCC (2007) strongly recommended that at least a 30-year period be employed for averaging GCM output data, to dampen the effects of inter-decadal variability. In our study, the base-line data for future land-use simulation is a 7-year period (from 1995 to 2002). In order to coincide with the climate change simulation, we followed the suggestion of IPCC (2007) and adopted four periods (28 years, approximate to 30 years) as a stage. Therefore, three predicted years in 2030, 2058, and 2086 represent the short-term, middle-term, and long-term land-use change. The predicted results are shown as Table 21. The prediction distinctly reveals that the building areas will increase from 13.36% in 1995 and 14.05% in 2002 to 38.91% in 2030, 52.13% in 2058, and reach 62.36% in 2086. Furthermore, the results obtained from Markov model and SEBAL model were combined to calculate the future CV values using equation (25) and (26), and shown as Table 22. From the results, the CV values for north Taiwan would reveal a decreasing trend no matter which storyline was

used.

Table 21. Predictions of land-use types in 2030, 2058, and 2086

Land-use types	2030	2058	2086
Forest	28.02%	22.58%	17.91%
Building	38.91%	52.13%	62.36%
Water	0.67%	0.50%	0.39%
Farmland	19.31%	14.95%	11.72%
Fallow farmland	13.09%	9.97%	7.79%
Total	100.00%	100.00%	100.00%

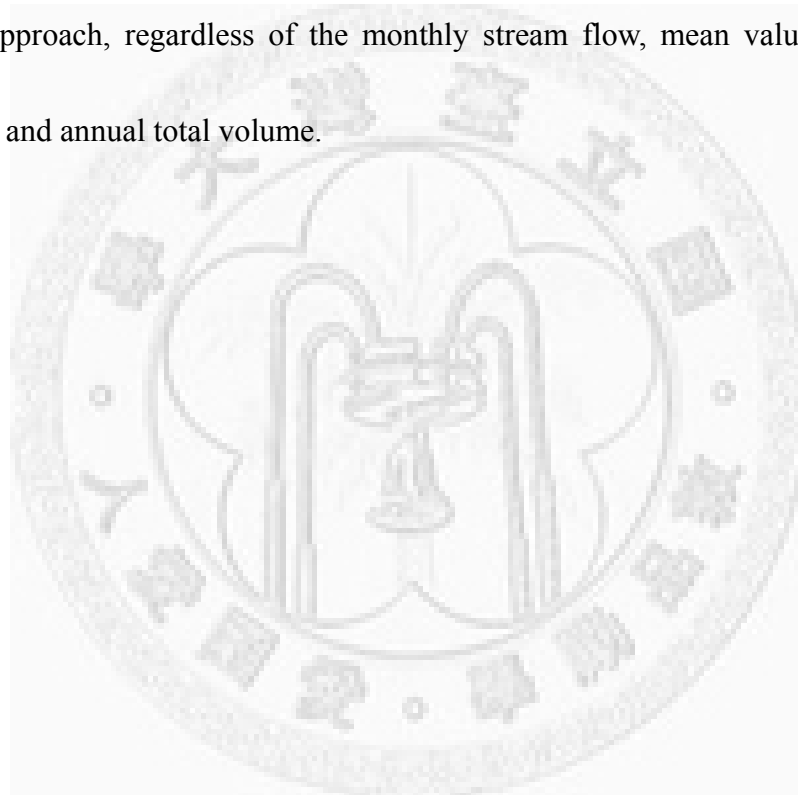
Table 22. Predictions of future CV values

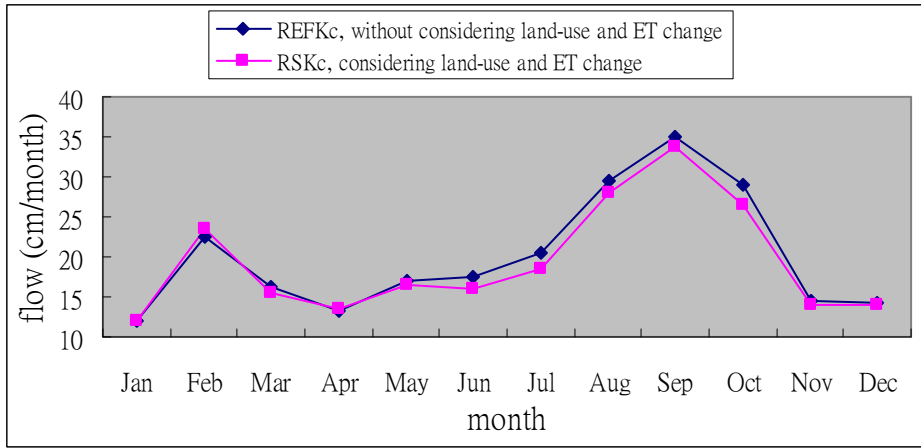
CV	2030	2058	2086
CV for wet season (A2 storyline)	0.997	0.896	0.813
CV for dry season (A2 storyline)	0.719	0.636	0.564
CV for wet season (B2 storyline)	1.000	0.902	0.813
CV for dry season (B2 storyline)	0.723	0.643	0.573

6.3.4. Effects of land-use change and ET change on future flow simulation

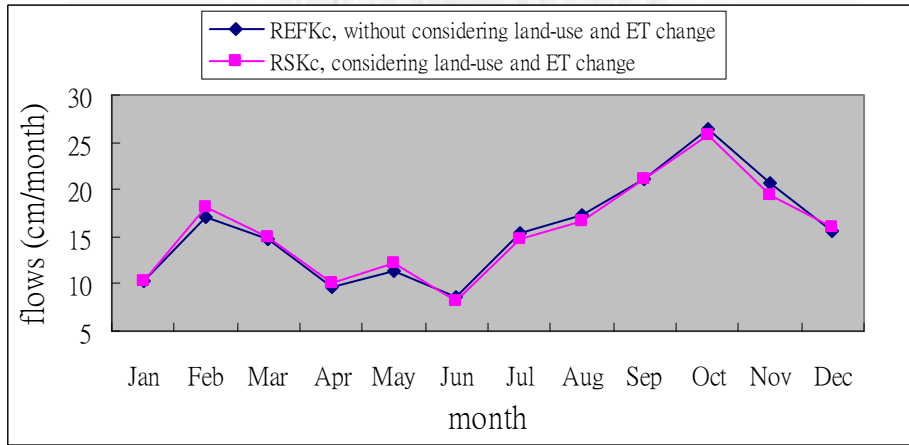
The future meteorological data was generated by using the CGCM1 modified predictors and weather generation model based on previous integrated weather records. Finally, flow series under short-term, mid-term and long-term climate change scenarios were projected using the GWLF model to assess the effects of land-use status and ET change on hydrological simulations. The two approaches to simulations were compared

in this step. Figure 19 compared the predicted stream flows between the traditional approach (*REFKc* parameter for current condition, without considering its future change) and proposed approach (*RSKc*, considering both land-use and ET change in the future). Table 23 represents the difference between the two simulations. The results revealed that the simulated flows using proposed approach were lower than those using traditional approach, regardless of the monthly stream flow, mean value of monthly stream flow, and annual total volume.

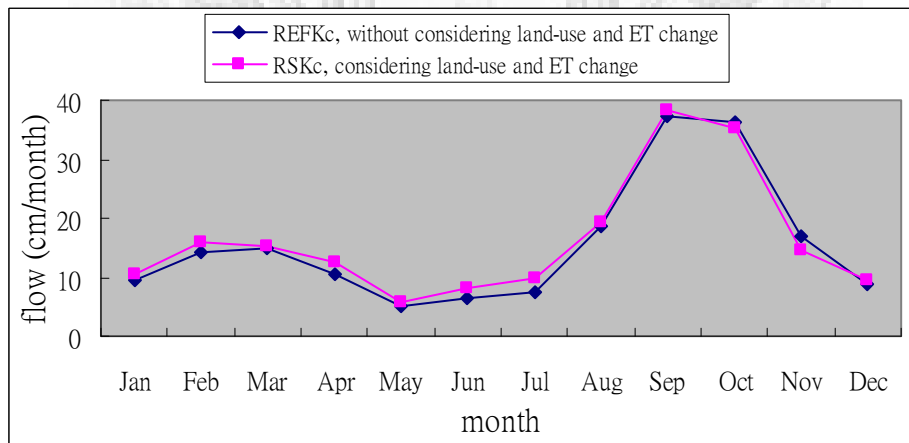




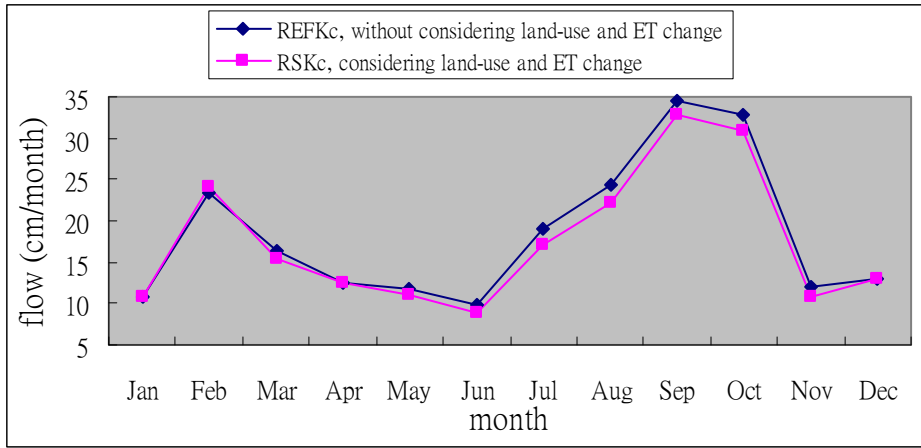
a



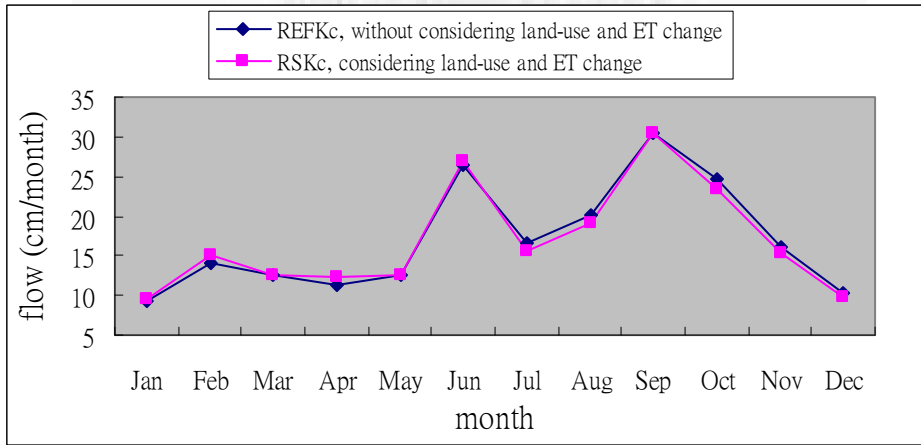
b



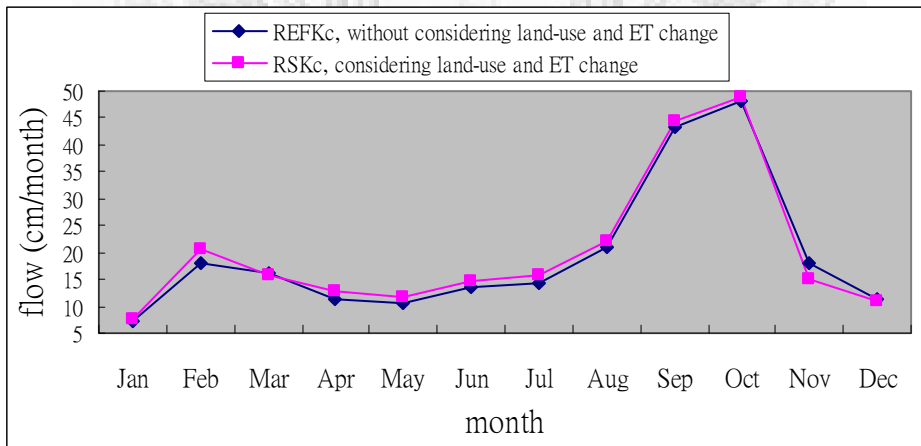
c



d



e



f

Figure 19. Comparison of the predicted stream flows between the traditional approach and proposed approach based on CGCM1 climate change model (a: A2, short-term; b: A2, middle-term; c: A2, long-term; d: B2, short-term; e: B2, middle-term; f: B2, long-term)

Table 23. Difference of stream flows (cm/month) between various approaches

Month	A2 Storyline			B2 Storyline		
	Short term	Middle term	Long term	Short term	Middle term	Long term
January	0.00	0.00	0.90	0.00	0.40	0.40
February	1.00	1.10	1.80	0.80	1.10	2.80
March	-0.90	0.20	0.40	-0.90	0.00	-0.40
April	0.30	0.50	1.80	0.10	1.00	1.30
May	-0.50	0.80	0.60	-0.60	0.00	1.20
June	-1.60	-0.40	1.90	-1.10	0.50	1.10
July	-2.00	-0.60	2.50	-2.00	-1.00	1.20
August	-1.50	-0.60	0.60	-2.20	-1.00	1.00
September	-1.40	-0.20	0.90	-1.70	0.10	1.40
October	-2.40	-0.70	-0.90	-1.90	-1.40	0.60
November	-0.70	-1.20	-2.50	-1.30	-0.80	-2.80
December	-0.20	0.50	0.70	0.00	-0.40	-0.10
Total	-9.90	-0.60	8.70	-10.80	-1.50	7.70
Average	-0.82	-0.05	0.73	-0.90	-0.12	0.64

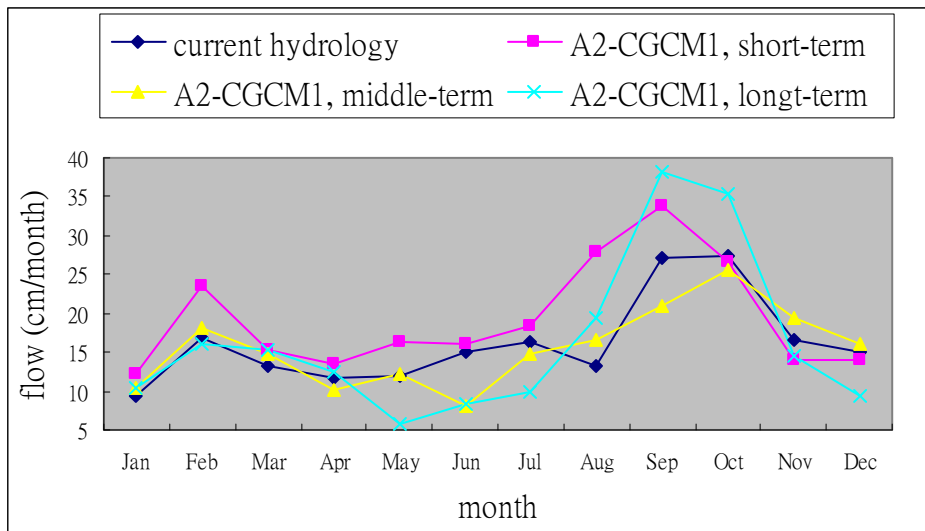
6.4. Investigation of Future Impact on Hydrological Cycle of North Taiwan

To further investigate how land-use change, ET change, and climate change affected river flows of north Taiwan, flow series from 1995 to 2002 (Table 24) was estimated to represent the current hydrological condition, and then compared with the future flows, the result was in Figure 20. Table 25 shows the value changes for future condition to the current condition. Positive values in the table denote an increase of flow, whereas negative values represent a decrease of flow. The results indicate that the overall values in future flow change have increasing trend. That is, the integrated effects

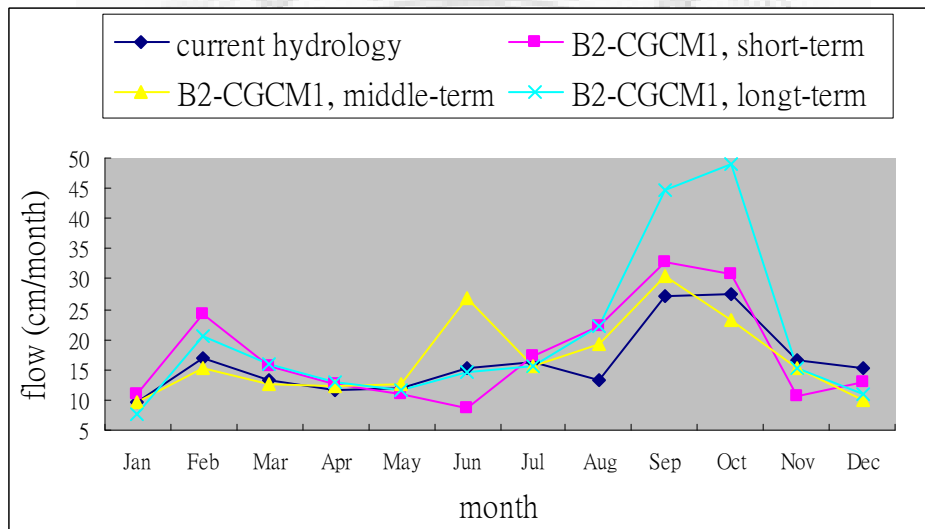
from urban sprawl, ET decline, and atmospheric changes would lead to an increase in the flow volumes of north Taiwan.

Table 24. Simulated flow values (cm/month) of north Taiwan under current condition

Month	Simulated flow values (Using <i>RSCV</i>)
January	9.5
February	16.9
March	13.2
April	11.7
May	12
June	15.1
July	16.2
August	13.2
September	27.2
October	27.4
November	16.7
December	15.1
Total	194.2
Average	16.2



a



B

Figure 20. Comparison of hydrographs between current and future conditions (a: SRES-A2 scenario; b: SRES-B2 scenario)

Table 25. Stream flow changes (cm) of north Taiwan due to land-use change, ET change and climate change

Month	A2 Storyline			B2 Storyline		
	Short term	Middle term	Long term	Short term	Middle term	Long term
January	2.6	0.8	0.9	1.3	0.1	-1.9
February	6.6	1.2	-0.9	7.2	-1.8	3.8
March	2.2	1.7	2.0	2.3	-0.7	2.6
April	1.9	-1.6	0.7	0.9	0.7	1.1
May	4.4	0.2	-6.2	-0.9	0.6	-0.4
June	0.9	-6.9	-6.8	-6.3	11.9	-0.4
July	2.2	-1.4	-6.2	0.9	-0.5	-0.6
August	14.8	3.4	6.2	9.0	5.9	8.9
September	6.5	-6.2	11.0	5.6	3.3	17.4
October	-0.9	-1.7	7.9	3.5	-4.1	21.5
November	-2.8	2.7	-2.1	-6.0	-1.4	-1.6
December	-1.0	0.9	-5.7	-2.2	-5.3	-4.0
Total	37.4	-6.9	0.8	15.3	8.7	46.4
Average	3.1	-0.6	0.1	1.3	0.7	3.9

7. DISCUSSIONS

7.1. Daily ET Difference among Various Land-use Types

1. In this study, a hybrid approach was applied to generate the land-use maps of north Taiwan. The examination of test area obtained a satisfactory result with the overall accuracy of 89.09%. However, the discrimination between spectral class and information classes was still problematic. For example, according to the national land-use inventory data, both farmland and fallow farmland are subclasses under agriculture land. During the image classification, farmland and fallow farmland can not be combined into one class because the two cover types have different characteristics of spectral reflectance. Thus, it becomes an important subject for further study to decide on the appropriate number of spectral classes coinciding with the classes categorized using information from actual field studies.
2. Ground land-use inventory is necessary for validating the accuracy of image classification. But acquiring ground truth data which has the same land types as the classification objective is difficult, particularly for intensive land use like Taiwan. In this study, the categories of the national land-use inventory data were firstly combined to coincide with those of remote sensing classification before the accuracy assessment. Certainly some errors may occur during the combination. But

with 89.09% overall accuracy, the result seems satisfactory. Further studies should be aware of the influence of the thematic difference between ground truth data and image classification on the accuracy assessment.

3. To validate the SEBAL simulations, the Pan ET records obtained from five weather stations (i.e., Taipei, Zhu-ZI-Hu, Ji-Long, Yi-Lan, and Xin-Zhu) on November 25, 1995 were regarded as ground truth data. An unpaired t-test was then applied to assess the difference between the field record and the simulated ET. The result showed that the calculated p value was 0.395, greater than 0.05. This result explains that there is no significant difference between the observed ET and the simulated ET. Therefore, the SEBAL model can be a feasible approach to estimate the ET on a large scale.
4. The main limitation of this and other studies relying on remote sensing technologies is that satellite image quality and land-use classification affect the estimations of actual ET and CV. In Taiwan, it is not easy to collect a clear image because of the weather, and shadow effects are also common due to a mountainous terrain. These two factors increase the difficulty of image classifications. To solve the problem, our study and most previous studies have opted to mask out the shaded areas of cloud and shadow before ET and CV were calculated. If clearer images become available in the future, they would be helpful in applying the SEBAL model. On the other

hand, SEBAL can potentially use other satellites images such as MODIS, AVHRR (Morse et al., 2000). These satellite images are able to provide more frequent observations to allow more frequent calculations of ET in addition to the large-scale analysis and the solution of cloud cover with Landsat data. Further studies can extend to this issue.

5. ET is a term used to describe the sum of “evaporation” and “plant transpiration” from the Earth's land surface to atmosphere. Evaporation accounts for the movement of water to the air from sources such as the soil, canopy interception, and waterbodies. Transpiration accounts for the movement of water within a plant and the subsequent loss of water as vapor through stomata in its leaves. In north Taiwan, seldom species of plant live on the water area. ET released from water surface usually involves only “evaporation”, no “transpiration”. However, the ET from the forest includes both “evaporation” and “transpiration”. A fully grown tree may lose several hundred gallons of water through its leaves on a hot, dry day. About 90% of the water that enters a plant's roots is used for this process (Cummins 2007; Martin et al. 1976). Chen et al. (2006) also showed the same result as our study. For above reasons, the ET value of forest can be higher than that of water.

6. The FAO paper of crop evapotranspiration (Allen et al. 1998) stated that: The CV should be adjusted for the local climate as indicated in Table 26. For this reason, the

value of actual ET might be greater than the potential ET due to the effect of wind speed. This effect also led to the value of CV could be higher than “one”. In fact, the SEBAL model also considered the wind effect, and in our study, information of wind speed was obtained from the weather stations (Table 27 and Table 28). Therefore, our results seem reasonable.

Table 26. CV for rice for various climatic conditions (Allen et al. 1998)

Humidity	Wind speed		
	light	moderate	strong
arid - semi-arid	1.10	1.15	1.20
sub-humid - humid	1.05	1.10	1.15
very humid	1.00	1.05	1.10

Table 27. Evapotranspiration cover coefficients for annual crops (Davis and Sorensen 1969; cited in Novotny and Chesters 1981; Haith et al. 1992) (only the value greater than “one” is shown)

Crop	Percent of Growing Season										
	0	10	20	30	40	50	60	70	80	80	100
Field corn	-	-	-	-	-	-	-	1.08	1.2	1.08	-
Grain sorgh	-	-	-	-	1.1	1.2	1.1	-	-	-	-
Wint wheat	1.08	1.19	1.29	1.35	1.4	1.38	1.36	1.23	1.1	-	1.08
Cotton	-	-	-	-	-	-	1.19	1.11	-	-	-
Sugar beets	-	-	-	-	-	-	1.08	1.26	1.44	1.3	-
Cantaloupe	-	-	-	-	-	-	1.05	1.22	1.13	-	-
Potatoes	-	-	-	-	1.06	1.24	1.4	1.5	1.5	1.4	-
Papago peas	-	-	-	-	1.04	1.16	1.26	1.25	-	-	-
Beans	-	-	-	1.05	1.07	-	-	-	-	-	-
Rice	-	1.06	1.13	1.24	1.38	1.55	1.58	1.57	1.47	1.27	-

Table 28. Evapotranspiration cover coefficients for perennial crops (Davis and Sorensen 1969; Novotny and Chesters 1981; Haith et al. 1992) (only the value greater than “one” is shown)

	Alfalfa Pasture	Grapes	Citrus Orchards	Deciduous Orchards	Sugarcane
January	-	1.16	-	-	-
February	-	1.23	-	-	-
March	-	1.19	0.15	-	-
April	1.02	1.09	-	-	1.17
May	1.08	-	-	-	1.21
June	1.14	-	-	-	1.22
July	1.2	-	-	-	1.23
August	1.25	-	-	-	1.24
September	1.22	-	-	1.08	1.26
October	1.18	-	-	1.03	1.27
November	1.12	-	-	-	1.28
December	-	-	-	-	-

7.2. Estimations of Environmental Parameters under Various Ecosystem Classification Systems and Spatial Scales

This study integrated the SEBAL model and Landsat thematic data to investigate the effect of ecosystem classification systems and spatial scales on environmental parameters. The results showed that spatial scales and ecosystem classification systems affected the estimation of environmental parameters. In fact, locality is also an influence on the characteristics of environmental parameters. This study only adopted north Taiwan for the empirical analysis, and did not consider the difference among various

regions of Taiwan (i.e. central, eastern, western, and southern Taiwan). It is suggested that further studies focus on the investigation of locality on environmental parameters in other regions.

7.3. Effects of Future Land-Use Status and ET Change on Stream Flow

Simulation

1. This study is novel in that it used an integration of the SEBAL model, the CGCM1 model, and the Markov model to estimate future land-use and ET parameters for stream flow simulations assuming a climate change scenario and then compared the simulated results with the traditional approach. Flow values derived from the proposed method were smaller than those using the traditional approach. Readers should be aware of some limitations regarding the numbers of CV used herein. In general, CV might vary in different seasons due to the effects of land cover change and vegetation growth. In addition, cloud effects are always a serious problem in Taiwan. For the above reasons, this study was able to apply only these two clear Landsat-5 images (July 20 and November 25, 1995) representing the CV of wet and dry seasons. When images from different months or seasons become available, certainly the monthly or seasonal *RSCV* values can be calculated using our remote sensing approach. Thus, it is suggested that further studies focus on the comparison

of the influence of CV at different months or seasons.

2. The CVs of the two approaches were higher than the reference CV from the traditional approach (wet season: 0.826; dry season: 0.754), even though the values applied in the proposed approach were decreasing due to the effects of land-use change such as urban and deforestation (see Table 22). Higher CV values indicate higher amounts of evapotranspiration, which would lead to the decrease of stream flows. This explains the differences of derived flow values between the proposed and traditional approaches.

3. In this study, the future CV values derived from the integration of the SEBAL model, the CGCM1 model, and the Markov model were based on the assumption that the ET of each land-use type would be invariable in the future. However, ET might be affected due to the change of forest structure (species, age) and urban composition (including more concrete building or vegetation). Readers should be aware of the fact that the accuracy of future CVs can be improved when the future ET values are available. Therefore, how to estimate the future ET values is an important issue for further study.

4. To predict future land-use status, the Markov model has the following assumptions.

(1) Land-use change of the study area is stable with no new disturbances; (2)

Transition probability remains consistent in the future. However, land-use is usually

a dynamic process. The transition probability might be variable due to the impacts of social or economical factors. For this reason, the uncertainty of land-use simulation should be considered before applying the Markov model.

7.4. Future Impacts on Hydrological Cycle of North Taiwan

Atmospheric and hydrological conditions are complex and highly changeable over time. The amounts of data are an unavoidable influence on trend analysis and the predicted changes of stream flow. Therefore, the collection of basic data records over a long period is necessary to improve the reliability of climate change simulations. This study was limited by the data acquisition and was able to use only eight years of records (from 1995 to 2002) from gauged weather and flow observations to assess the effect of climate change on hydrology.

8. CONCLUSIONS

This study focused on an integrated analysis of the hydrological cycle in north Taiwan using remote sensing. Three kinds of models such as the SEBAL model, the GWLF model, and the CGCM1 model were integrated with the purposes of estimating the daily ET among various land-use types; the effects of ecosystems classifications and spatial scales on environmental parameters; the potential effects of land-use change and ET change on future stream flow simulations; and the assessment of future impacts on the hydrology of north Taiwan. The main conclusions of the study are as follows:

1. Using the hybrid classification method and Landsat-5 images, the generated land-use maps of the study area were classified into seven categories including forest, buildings, farmland, fallow farmland, water, cloud, and shadow. The accuracy of land-use classification evaluated by test areas was 89.09%. This implies that hybrid classification is a useful approach to generate a land-use map. In turn, the generated land-use maps are suitable for estimating the CV and actual ET.
2. The values of energy balance parameters among various land-use types were different. Forestland had higher values with NDVI and actual ET, and had lower values of surface temperature, soil heat flux and sensible heat flux. The calculated parameters conformed to our expectations that surface temperature, NDVI and

actual ET had higher values in July, and sensible heat flux and soil heat flux had higher values in November. Similarly, the mean daily ET in July (0.531 cm/day) was higher than in November (0.233 cm/day). Meanwhile, the ET values derived from the SEBAL model were different among different land-use types. For example, in this study, forest has larger ET (January: 0.723cm; November: 0.395cm) than building (January: 0.220cm; November: 0.088cm).

3. Environmental parameters among various land-use types were different among five land-use types, and the required parameters and the numbers of parameters for discriminating five land-use types were also different under different ecosystem classification systems at various scales. However, NDVI and emissivity seem to be the most significant parameters no matter what the kind of spatial scales and ecosystem classification systems.
4. The calculations of CV using two approaches have large differences in different seasons. For example, the calculated CV for the wet season (*RSCV*: 1.245; *REFCV*: 0.842) was higher than the value of the dry season (*RSCV*: 0.851; *REFCV*: 0.717). Moreover, the overall trend of CV values derived from remote sensing techniques (July 20: 1.245; November 25: 0.851) were larger than the CV of the traditional approach (July 20: 0.842; November 25: 0.717). This result affected the stream flow simulations.

5. The assessment of CV effects on stream flow simulation indicated that, the flows obtained from *RSCV* were more accurate than that from *REFCV*, regardless of the monthly stream flow, the mean value of monthly stream flow, and the annual total stream flow from 1995 to 2002. The regression analysis also pointed out that the flow simulation using *RSCV* (regression coefficient = 0.877) would represent truer flow characteristics than the use of *REFCV* (regression coefficient = 0.853).
6. Goodman's Chi-squared statistic indicates that the procedures of land-use change during 1995 to 2002 were not random. The prediction of overall land-use status from 1995 to 2002, 2030, 2058, and 2086, respectively showed that the building area increased rapidly from 13.36% in 1995 and 14.05% in 2002 to 38.91% in 2030, 52.13% in 2052, and 62.36% in 2086. The predicated CV values for next three periods revealed a decreasing trend no matter which climatic change storyline was chosen.
7. Flow simulations were affected by the predicted future land-use change and ET change. Regardless of the monthly stream flow, mean value of monthly stream flow, and annual total stream, the predicted flows considering land-use change and ET change were lower than those calculated without considering the two effects.
8. Impact assessment of north Taiwan hydrology indicated that, even though some values were reduced, the overall results predicted a raising tendency for future flow

change. That is, That is, the impacts of urban expansion, ET decline, and climate change will increase the flow volumes.

The conclusions summarized from this study indicate that land-use type and spatial scales affected the estimation of ET, and their effects can be investigated by integrating remote sensing techniques, SEBAL model and multivariate statistical analysis. Stream flow simulation using remote sensing-based CV could present truer hydrological characteristics than the traditional approach. The integration of the SEBAL model, the CGCM1 model, and the Markov model is also a feasible scheme to estimate the future land-use status and CV values for stream flow. The consideration of land-use change and ET change indeed affects the predicted flows. The results of the hydrology analysis based on the SRES scenarios of CGCM1 model predicted that the river flows of north Taiwan will become greater due to the effects of climate change, land-use change and ET change. Therefore, the results obtained from this study can be extrapolated to the future studies of global environmental change and water resource management.

REFERENCES

Aaviksoo K (1995) Simulation vegetation dynamics and land use in a mire landscape using a Markov model. *Landscape Urban Plan* 31:129–142.

Allen RG, Pereira LS, Raes D, Smith M (1998) Crop evapotranspiration-Guidelines for computing crop water requirements - FAO Irrigation and drainage paper 56. FAO corporate document repository. <http://www.fao.org/docrep/X0490E/x0490e00.htm>. Accessed 10 November 2009.

Anderson JR, Hardy EE, Roach JT, Witmer RE (1976) A land use and land cover classification system for use with remote sensor data. U.S Geological Survey, Washington, pp 8-10.

Arnell NW, Reynard NS (1996) The effect of climate change due to global warming on river flow in great Britain. *Journal of Hydrology* 183:397–424.

Bailey RG (1996) *Ecosystem Geography*, Springer, New York, 1-49.

Bastiaanssen WGM, Menenti M, Feddes RA, Holtslag AAM (1998a) A remote sensing surface energy balance algorithm for land (SEBAL): Part 1 formulation. *Journal of Hydrology* 212–213:198–212.

Bastiaanssen W.G.M, Pelgrum H, Wang J, Ma Y, Moreno J, Roberink GJ, van der Wal, T (1998b) A remote sensing surface energy balance algorithm for land (SEBAL):

Part 2 Validation. *Journal of Hydrology* 212-213: 213-229.

Bosen JF (1960) A formula for approximation of saturation vapor pressure over water.

Monthly Weather Reviews 88(8): 275–276.

Burnham BO (1973) Markov intertemporal land use simulation model. *Southern J. of*

Agri. Econ 5:253–258.

Chang PJ (2008) A study of the influence of climate change on farmland suitability of

paddy. (Thesis for Master of science), National Taipei University, Graduate School of Real Estate and Built Environment, p 108. (in Chinese, with English abstract).

Chen MY (2002) Study of Water Resources System Dynamics Model and Sustainable

Management Strategies for the TanShui River Watershed. (Thesis for Master of science), National Taiwan University, Department of Bioenvironmental System Engineering, Taipei, Taiwan, p109. (In Chinese with English abstract)

Cheng CC, Chen, YK, Jan JF, Wang SF (2005) DTM, GIS, and DSS applications in

forestland ecosystem classification and suitability analysis. *Journal of Photogrammetry and Remote Sensing* 10:351-360.

Cheng CC, Hsu LT, Wu CD (2006) Monitoring forest landscape using photogrammetric

techniques and landscape models. The 27th Asian Conference on Remote Sensing, Ulaanbaatar, Mongolia.

Cheng CC, Lo HC, Chen YK, Wu CD (2008) Assessment of ecosystem classification

systems at various spatial scales on environmental parameters using remote sensing techniques. *Journal of Photogrammetry and Remote Sensing* 241–254.

Cheng CC, Wu CD, Chuang YC (2007) Influence of land-use changes and climate change on stream flow simulations: a case study of the Jiao-Long watershed. *Taiwan Journal of Forest Science* 22(4):483–495. (in Chinese, with English abstract).

Cheng CC, Wu CD, Wang SF (2005) Application of Markov and Logit Models on Monitoring Landscape Changes. *Taiwan J For Sci* 20(1):29–36.

Chen CT, Wu ST, Chiang YF (2006) Using MODIS satellite images to estimate evapotranspiration in Taiwan. *Taiwan Journal of Forest Science* 21(2):249–261

Chiou YL (1995) The observation and analysis of evapotranspiration in land process. (Thesis for Master of science), Graduate Institute of Hydrological and Oceanic Sciences, National Central University, Tao-Yuan, Taiwan, 95p. (in Chinese, with English abstract).

Cummins B (2007) *Biological science*, 3rd edn. Scott, Washington, pp 215.

Davis CV, Sorensen KE (1969) *Handbook of applied hydraulics*. McGraw–Hill, New York.

Douglas AH, Shoemaker IL (1987) Generalized watershed loading functions for stream flow nutrients. *Water Resources Bull* 107:121–37.

- Fan CC (1998) The impacts of climate changes on groundwater recharge in Taiwan. (Thesis for Master of science), Graduate Institute of Agricultural Engineering, National Taiwan University, Taipei, Taiwan. (in Chinese, with English abstract).
- Flato GM, Boer GJ, Lee WG, McFarlane NA, Ramsden D, Reader MC, Weaver AJ (2000) The Canadian centre for climate modeling and analysis global coupled model and its Climate. *Climate Dynamics* 16:451–467.
- Giertz S, Junge B, Diekkruger B (2005) Assessing the effects of land use change on soil physical properties and hydrological processes in the sub-humid tropical environment of West Africa, *Physics and Chemistry of the Earth* 30:485-496.
- Goodman LA (1968) The analysis of crossclassified data: Independence, quasi-independence, and interactions in contingency tables with or without missing entries. *J. Am. Stat Assoc* 63:1031–1091.
- Haith DA, Mandel R, Wu RS (1992) Generalized watershed loading functions version 2.0 user's manual. Department of Agricultural and Biological Engineering, Cornell University, Ithaca, New York.
- Haith DA, Shoemaker LL (1987) Generalized watershed loading functions for stream flow nutrients. *Water Resources Bulletin* 23(3):471–478.
- Hamon WR (1961) Estimating potential evapotranspiration. *Proceeding of the American Society of Civil Engineers. Journal of the Hydraulics Divison* 87(HY3): 107-120.

Hillier FS, Lieberman GJ (1995) Introduction to operations research. Mcgraw-Hill International.

Hoffer RM, Fleming M (1978) Mapping vegetative cover by computer-aided analysis of satellite data, Purdue University, LARS Technical Report 011178.

Hong NM (1997) The impacts of climate change on the management of water resources in the Ta-An River. (Thesis for Master of science), National Taiwan University, Department of Bioenvironmental System Engineering, Taipei, Taiwan. p 67. (in Chinese, with English abstract)

Hsieh LS, Liu WC, Tung, CP (2001) A Study of the Potential Impact of Climate Change on the Flood Protect System for Da-Han Stream and Shih-Dan Stream. Chinese Journal of Agricultural Engineering, 50(3): 32-47. (In Chinese with English abstract).

Hsu LT, Cheng CC (2000) Assessing landscape change in Liukuei ecosystem area using Markov model. Taiwan J For Sci 15(1):41-9.

Huang YM (2008) A study on the evapotranspiration of Taoyuan area. (Thesis for Master of science), Chinese Culture University, The Department and Graduate Institute of Landscape Architecture, Taipei, Taiwan, p 79. (in Chinese, with English abstract).

IPCC (2002) Special report on emissions scenarios.

<http://www.ipcc.ch/ipccreports/sres/emission/index.htm>

IPCC (2004) 16 years of scientific assessment in support of the climate convention.

<http://www.ipcc.ch/pdf/10th-anniversary/anniversary-brochure.pdf>

IPCC (2007) Climate change 2007, Working Group III (WGIII) mitigation of climate

change. <http://www.ipcc.ch/ipccreports/ar4-wg3.htm>

Knapp HV (1985) Evaporation and Transpiration. In Handbook of Applied Meteorology.

ed. D.D. Houghton, Wiley, New York, NY, pp 537-554.

Lang R, Shao G, Pijanowski, BC Farnsworth RL (2008) Optimizing unsupervised

lassifications of remotely sensed imagery with a data-assisted labeling approach,

Computer and Geosciences 34:1877-1885.

Laymon C, Quattrochi D, Malek E, Hipps L, Boettinger J, McCurdy G (1998)

Remotely-sensed regional-scale evapotranspiration of a semi-arid great basin

desert and its relationship to geomorphology, soils, and vegetation.

Geomorphology 21:329–349.

Li MH, Tung CP, Sui CH, Yang, FH (2006) Estimating seasonal basin rainfall using

tabu search. Terrestrial, Atmospheric and Oceanic Sciences 17(1)295–316.

Liang S (2000) Narrowband to broadband conversions of land surface albedo - I

Algorithms, Remote Sensing of Environment 76:213-238.

Lillesand TM, Kiefer RW (2004) Remote sensing and image interpretation, fifth edition,

Wiley, New York, NY, 763p.

Lindsay BE, Dunn DL (1979) Land use projections under alternative policies: a transition matrix approach. *Journal of the Northeastern Agricultural Economics Council* 8(2):87–99.

Lo CP, Choi J (2004) A hybrid approach to urban land use/cover mapping using Landsat 7 Enhanced Thematic Mapper Plus (ETM+) images. *Int. J. Remote Sensing* 25(14):2687–2700.

Markel D, Somma F, Evans BM (2006) Using a GIS transfer model to evaluate pollutant loads in the Kinnere watershed, Israel. *Water Science and Technology* 53(10):75-82.

Manning M, Nobre C (2001) *Climate change 2001: impacts, adaptation, and vulnerability*. IPCC working group II. United Kingdom.

Martin J, Leonard W, Stamp D (1976) *Principles of field crop production*, 3rd. Macmillan, New York.

Martinez-Casasnovas JA (2000) A cartographic and database approach for land cover/use mapping and generalization from remotely sensed data, *International Journal of Remote Sensing* 21(9):1825-1842.

Mausser W, Scha'dlich S (1998) Modeling the spatial distribution of evapotranspiration on different scale using remote sensing data. *Journal of Hydrology* 212-213: 250-267.

Menenti M, Choudhury BJ (1993) Parameterization of land surface evaporation by means of location dependent potential evaporation and surface temperature range. In Proc. Exchange processes at the land surface for a range of space and time scales. IAHS Publ, 212, pp 561–568.

Morse AT, Tasumi G, Richard A, Willam JK (2000) Application of the SEBAL methodology for estimating consumptive use of water and stream flow depletion in the bear river basin of Idaho through remote sensing. The Raytheon Systems Company-Earth Observation System Data and Information System Project, Waltham, M A.

Muller MR, Middleton K (1994) A Markov model of land-use change dynamics in the Niagara region, Ontario, Canada. *Landscape Ecology* 9: 151–157.

Nakicenovic N, Swart R (2000) Special Report on Emissions Scenarios (SRES). IPCC Special Report. Cambridge University Press. UK.

Novotny V, Chesters G (1981) Handbook of nonpoint pollution. Van Nostrand Reinhold, New York.

Oberg J, Melesse AM (2004) Evapotranspiration changes at the glacial ridge prairie wetland restoration project: A remote sensing perspective. In: Proc. of self-sustaining solutions for streams, wetlands and watersheds, ASAE Specialty Conference, September 12–15 2004, St Paul, Minnesota.

Parry M, Canziani O, Palutikof J, Linden Pvd, Hanson C (2007) Climate change 2007: impacts, adaptation, and vulnerability. IPCC working group II. Cambridge University Press. UK.

Pickering NB, Stedinger JR, Haith DA (1988) Weather input for nonpoint source pollution models. *Journal of Irrigation and Draining Engineering* 114(4) 674–690.

Rao PK, Holmes SJ, Anderson RK, Winston JS, Lehr PE (1990) Weather satellites: Systems data and environmental applications American meteorological society. Boston 503p.

Su HJ (1992) Vegetation of Taiwan: altitudinal vegetation zones and geographical climatic regions, *Proceedings of the workshop on the Biological Resources and Information Management of Taiwan* 39-53. (in Chinese, with English abstract).

Tien WT (2003) The effects of climate change on the land hydrologic cycles in Taiwan. (Thesis for Master of science), National Central University, Graduate Institute of Hydrological and Oceanic Sciences, Taoyuan, Taiwan, p105. (in Chinese, with English abstract).

Tokumar K, Kogan FN (1993) Satellite technology for environmental monitoring in developing countries, United Nations Educational, Scientific and Cultural Organization. Paris 51-89.

Trezza R (2002) Evapotranspiration using a satellite-based surface energy balance with

standardized ground control. Ph.D. Dissertation, Utah State University, Logan, UT.

Tung CP (2001) The Impacts of climate change on Tsengwen creek water resources in Taiwan. *Journal of American Water Resources Association*. 37(1):1-10.

Tung CP, Haith DA (1995) Global warming effects on New York stream flows. *Journal of Water Resources Planning and Management* 121(2):216–225.

Tung CP, Wu MC, Chen SC (1999) Influence of spatial resolution and doubled CO₂ on hydrologic simulations over Taiwan. 1st International RSM Conference. Maui, Hawaii, USA, July 1999.

Turner MG (1993) Landscape changes in nine rural counties in Georgia. *Photogram Eng Remote Sensing* 56(3):379- 86.

Weiler M, Jost G, Gluns D, Green K, Alila Y (2005) Designing experimental watersheds to understand and quantify the influence of land-use management and natural variability on the hydrological response at multiple scales. *Headwater 2005*, June 2005, Bergen, Hordaland, Norway, *Headwater 2005*.

Wolf A, Lawrence B, Lowry R, Dam KKV, Cramer K, Gutierrez M, Kondapalli S, Latham S, O'Neill S, Stephens A (2005) Climate science modelling language: standards-based markup for metocean data, 85th meeting of American Meteorological Society, San Diego.

Wu CD (2004) Monitoring of landscape change on unlawful cultivated forestland.

(Thesis for Master of science), National Taiwan University, Graduate Institute of Forestry, Taipei, Taiwan. (in Chinese with English summary).

Wu RS, Haith DA (1993) Land use, climate and water supply. *Journal of Water Resources Planning and Management* 119(6):685-704.

Yang X, Lo CP (2002) Using a time series of satellite imagery to detect land use and land cover changes in the Atlanta, Georgia metropolitan area. *International Journal of Remote Sensing* 23:1775–1798.

Yu PS, Yang TC, Wu CK (2002) Impact of climate change on water resources in southern Taiwan. *Journal of Hydrology* 260:161-175.

